Study on Carbothermal Reduction Process from Alumina to Aluminum

アルミナからアルミニウムへの炭素熱還元プロセスの研究

Amina Chahtou

Doctoral Program in Materials Processing Physics

Submitted to Departement of Science and Technology
On August 2018
in Partial Fulfillment of the
Requirements for the Degree of Doctor of Philosophy in
Science
(Advanced Materials Science and Technology)

At Graduate School of Science and Technology

Hirosaki University

Abstract

Recently, the world consumption of metal aluminum knew a significant rise. This growth in the demand is mainly due to the world focus on using a stable and lightweight material for automobiles, infrastructures and sensors technology. However, the conventional process known as Hall-Héroult used for the production of aluminum expresses a high energy cost and loss of greenhouse emissions. To deal with the high-cost problem, a substitution method known as the carbothermal reduction of alumina based on reducing the alumina with carbon as reductant material in an induction heating furnace shows to be efficient and expressed low energy cost. In the other hand, the yield of produced aluminum via carbothermal reduction of alumina still quite low. To improve the reduction process yield, the knowledge and study of the different processes occurring during the reduction are necessary to improve the efficiency of the carbothermal method and increase the yield of the final aluminum product. In the following, I describe the main objective of my study:

- Simulation and analysis of the phase stability diagram of Al-O-C, to understand thermodynamically the different reactions occurred during the carbothermal reduction process.

- Evaluation of the optimum heating temperature condition to achieve a higher yield based on the relationship between the partial pressure of the by-product gas-form (Al_2O and CO).

- Investigation of the effect of adding aluminum carbide to the starting raw materials mixture of alumina and carbon to speed up the reactions and enhance the reduction yield.

In this study, I have attempted to optimize and enhance the yield of the produced aluminum following all the objectives cited above and success on determining the optimum thermodynamics conditions such as the mole fraction, the pressure and the

temperature for the enhancements of the carbothermal reduction process yield. In addition, the positive effect of the additive on the improvement of the reduction process yield will be discussed in details..

The thesis is composed of four chapters. The first chapter is dedicated to discussing a brief history of aluminum production, with the importance of aluminum in the automobile and current industries. Furthermore, the current aluminum world market and the conventional process will be discussed. While the in the second chapter the direct carbothermal reduction of alumina compared to the conventional Hall-Heroult process will be explained in details including the thermodynamics theoretical background on the presence and stability of alumina, aluminum, aluminum carbide and carbon under various conditions such as temperature and pressure which are the key for the understanding of the reduction process. While all the focus of this research work is about the necessity optimization and precise determination of the heating process temperature which has a significant impact on the by-product Al_2O gas generation. On the other hand, the investigation of the aluminum carbide additive effect will be discussed in details to determine precisely its impact on the enhancement of the reduction process yield.

The third chapter will present the experimental procedures used for the two main work of this research starting with the optimization of the heating temperature for the reduction process. A complete explanation of its relationship to the stability phase diagram of Al-O-C, the material used and the effect on the final yield of the reduction. A second part, the experimental procedure of the aluminum carbide additive optimization such as the used material and methods, and the impact of the additive on the different reaction inside the process will be discussed. As for both experimental parts, the same characterization techniques will be used including XRD for product quantification and mass balance calculation, while Quadrupole mass spectroscopy (Q-mass) will be used for real-time estimation of different gas phase during the reduction process.

Chapter four will present the experimental results and discussions following each experimental procure discussed in the third chapter. The optimization results or the heating process temperature will be discussed in details with their impact on the determination of the exact temperature allowing a higher aluminum yield. While for the optimization of the aluminum carbide additive effect by comparing nine different ratios will be compared in term of gas loss, product composition, aluminum carbide and aluminum yield.

Finally, the conclusion section will summarize the achievement and comments on the investigation and enhancement of the carbothermal reduction of alumina for production of aluminum.

Acknowledgments

Table of contents

List of Abbreviation and Symbols

Abbreviation

wt%   weight percent

ppm   part per million

Q-mass   Quadrupole Mass Spectroscopy

XRD   X-ray Diffraction

Symbols

Al_2O_3 Alumina

Al_2O Silicon monoxide gas

CO Carbon monoxide gas

Al Aluminum

C Carbon

Al_3C_4 Aluminum Carbide

Al_4O_4C Aluminum Oxy-carbide

P_{CO} Partial Pressure of CO gas

P_{Al2O} Partial Pressure of SiO gas

s   Solid

l   Liquid

g   Gas

$NaF\text{-}AlF_3$ Sodium Aluminum Fluoride

List of Tables

List of Figures

Fig. 12 schematic comparison between current industrial process and carbothermic reduction process for the production of aluminum: (a) Hall-Héroult Electrolytic process and (b) our optimized carbothermic reduction process

Fig. 13 thermodynamic calculation of phase stability diagram of Al_2O/CO gas phases for reactions in Eq. (12) and in Eq. (14), calculated with data from MALT2. P_a and P_b correspond to the partial pressure ratio $P(Al_2O)/P(CO)$ as shown in Table 5

Fig. 14 real figure of the experimental apparatus. The carbon crucible was surrounded by thermal insulator (carbon felt) and quartz tube as electrical insulation

Fig. 15 typical temperature profile measured by the infrared thermometer during the reduction process. The lower limit of the infrared thermometer detection cannot measure the temperature below 925K.

Fig. 16 Functioning Principle of quadrupole mass spectrometry

Fig. 17 Schematic illustration of the Data Keylogger operation principle

Fig. 18 Real image of the Planetary Micro Mill Pulverisette 7

Fig. 19 Real image of the DRX SmartLab, Rigaku Corporatio

Fig. 20 X-ray diffraction patterns of obtained products using silicon for internal standard calibration.

Fig. 21 Calibration curve used in the internal standard method calculation.

Fig. 22 The heating temperature profiles recorded for different samples measured at the surface of the crucible cap via an infrared thermometer during the reduction process. The recording starts at 650°C (923K) due to the limit in the detection range of the infrared thermometer from 650°C to 3500°C

Fig. 23 Mass spectra of the chamber gases during the heating in case of six heating temperature profile. The amount of CO gas increased with increasing the temperature. However, the highest produced amount was achieved for a heating temperature of 1750 ºC in the sample (5)

Fig.24 X-ray diffraction patterns of obtained products for different heating-temperature profiles.

Fig.25 Total Al_4C_3 and lost gas yield obtained from all samples.

Fig. 26 Photos of the reduction product with six heating-temperature profiles. The color of the obtained product in each image exhibits approximately the containing elements of each occurred reaction

Fig. 27 Real-time evolution of the released CO gas during the reduction process analyzed by quadrupole mass spectrometry. The background gas of N_2 is represented below the dashed line. The factor k was used for the calculation of Al_2O (mol) gas loss

Fig. 28 X-ray diffraction patterns of obtained products in the case of various additives (0 ~0.1 mol%) of Al_4C_3

Fig. 29 Total Al yield obtained from all samples. The percentage of Al yield from Al_4C_3 was estimated. The highest Al yield was obtained in sample 5 where 0.05 mol% of Al_4C_3 was used.

Fig. 30 Total Al_4C_3 and gas lost yield obtained from all samples

Fig.31 Morphology of the samples observed (**a**) sample 1 without Al_4C_3 additive (**b**) sample 5 with 0.05mol% of Al_4C_3 additive (**C**) sample 9 with 0.1mol% of Al_4C_3 additive.

Fig.32 EDS mapping of particles morphology (**a**) sample 1 without Al_4C_3 additive (**b**) sample 5 with 0.05mol% of Al_4C_3 additive (**C**) sample 9 with 0.1mol% of Al_4C_3 additive.500μm

Fig.33 EDS mapping of particles morphology (**a**) sample 5 with 0.05mol% of Al_4C_3 additive (**b**) sample 9 with 0.1mol% of Al_4C_3 additive. 10μm

Chapter I. Introduction

Aluminum metal is a durable, lightweight material expressing when freshly cut a silvery color. It is known for its excellent heat and electricity conduction with the advantage of easy modeling and put to shaps. Two advantages of aluminum metal can be cited when compared with other metals.

At first, aluminum has a low density compared to iron and copper, about one third the density of iron and copper. Moreover, although it reacts rapidly with the oxygen in the air, it forms a thin tough and impervious oxide layer which resists further oxidation. These properties remove the need for surface protection coatings such as those required with other metals, in particular with iron.

Table 1 *Typical properties of aluminum*

Property	Value
Atomic Number	13
Atomic Weight (g/mol)	26.9815
Valency	3
Crystal Lattice	Face-centered cubic
Melting Point (°C)	660.2
Boiling Point (°C)	2480
Mean Specific Heat (0-100°C) (cal/g.°C)	0.219
Thermal Conductivity (0-100°C) (cal/cms. °C)	0.57
Co-Efficient of Linear Expansion (0-100°C) ($x10^{-6}$/°C)	23.5
Electrical Resistivity at 20°C ($\mu\Omega$cm)	2.69
Density (g/cm^3)	2.6898
Modulus of Elasticity (GPa)	70
Poissons Ratio	0.34

I.1 Brief history on the production of aluminum

Aluminum was one of the newest metals to be discovered by humans, which doesn't exist in its pure form in nature. Therefore, its discovery was late until the 19th century with the developments in chemistry and the advent of electricity [1].

In 1886, two scientists, Hall and Héroult, working independently, developed and patented a new process for direct electrolytic decomposition of aluminum oxide (Al_2O_3) [2], that would become the only method used today. The Hall-Héroult process was enhanced with the evolution of the Bayer process [3] which produces aluminum oxide from bauxite, which is used in the Hall-Héroult process. When the Hall-Héroult process was developed, the aluminum industry was born, and this process of extracting aluminum from its ore has been able to withstand many years and attempted to rewrite or add to it and remains the fundamental basis of all commercial aluminum production today.

Aluminum production processes used today are based on the Bayer and Hall-Héroult processes [4,5]. The aluminum industry was created over several decades. The story of the 'clay silver' came to an end, and aluminum became a new industrial metal.

Aluminum production was growing steadily worldwide and reached 19 millions tons by the beginning of the 1990s [6]. The role of China started to become more critical with the center of the world's production gradually drifting to its territory. Domestic aluminum production in China at the time did not exceed 900 thousand tons, but it was overgrowing, supplying their own needs.

The aluminum production facilities in Russia reached an annual production of 3.5 million tons [7]. However, the unstable situation of the country at the moment following its separation from the Soviet Union led to a significant decayed in its economy. The various changes in the economy model of Russia led a slow growth of the aluminum production.

China's production grew past Russia's in 2002 exceeding 4.3 million tons. 26 million tons of aluminum were produced worldwide at that time [8]. Hereafter, aluminum production in China grew at priority rates. It reached almost 10 million tons by 2006, one-third of total global production volumes.

In China, the aluminum was produced all self-consumed within the country walls. The turnaround of the metal and other materials were so significant that they led to emerging of Shanghai Futures Exchange ("SHFE") as a commodity exchange in 1999 [9]. At the same time, China ramped up its production at a high environmental price. More than 90% of the power used for aluminum production is generated from coal-burning stations[10]. Comparing to Russia, the situation was opposite in which hydraulic energy generates about 90% of the energy used for aluminum production[11]. The Countries in the Middle East also started to play a significant part in the aluminum industry. Their access to cheap oil and natural gas prices led to a cheap source but environmentally harmful power for aluminum production[12]. They also ramped up their production vigorously and today rank among the world leaders in the production of the winged metal.

Challenges for the world aluminum industry began in 2008 during the global financial crisis. The aluminum industry faced for the first time in its history overproduction phenomena caused by the collapse of the stock market. The consequences of this crisis led to a drop of 50% in aluminum price. Millions of tons of aluminum accumulated in storage facilities worldwide. Exchange traders showed interest in them, financial deals with the metal became a profitable investment [13].

2008-2009 crisis led to a significant closure of smelters owned by all Western aluminum companies. In the other hand, the production of aluminum continues its growth in the world. Producers such as China and the Middle East moved in the opposite direction by increasing their production of aluminum metal.

In 2013, the global aluminum industry made new gains with production exceeding 50 million tons. The growth in the aluminum consumption used in urbanization and industrialization led to further development of the aluminum industry. Aluminum will be more actively replacing heavier steel in the automotive industry and a more expensive copper in electrical engineering. According to forecasts, the demand for aluminum will exceed 80 million tons by 2020 as shown in Fig. 1.
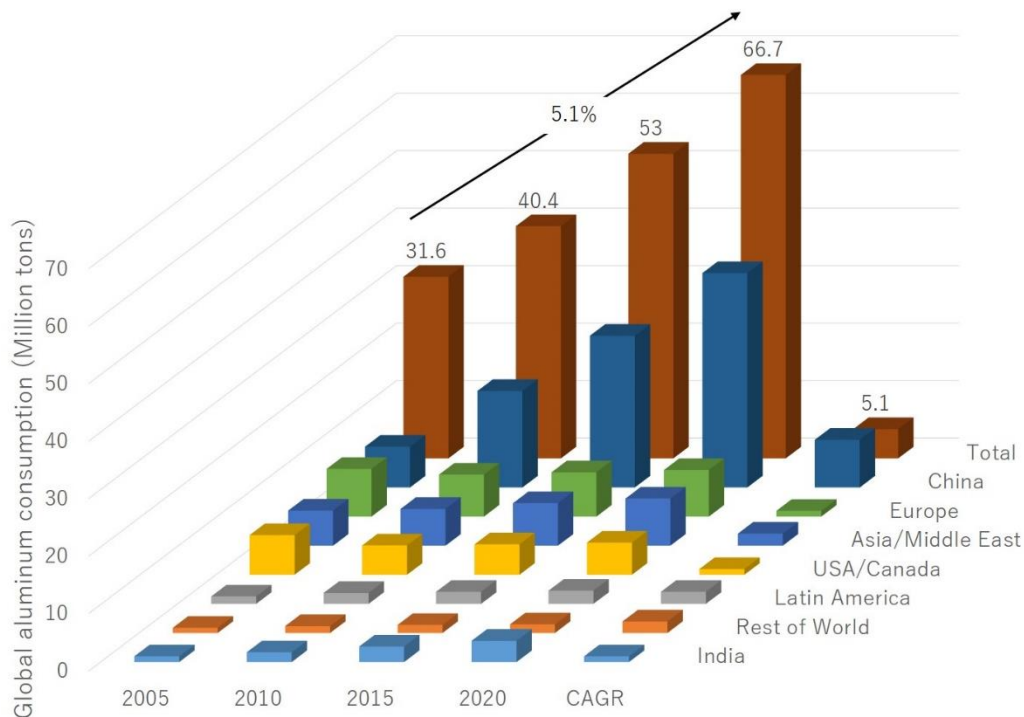
Fig. 1 Global aluminum consumption and prediction from 2005 to 2020.

I.2 Worldwide usage of aluminum

Aluminum metals represent one of the most important and needed metals used by modern society. It is indispensable with various structural materials in automotive, aviation industries (transport), construction and electrical engineering [14]. However, with machinery and equipment, foil stock and packaging, consumer durables and other accounted less than the others. Fig. 2 shows most of the worldwide aluminum consumption is fabricated from aluminum source, primarily due to its durability and its third most abundant element in the world. Aluminum is an excellent thermal property and

resistance to corrosion have led to its use in air conditioning, refrigeration, and heat-exchange systems. Finally, its malleability has allowed it to be rolled and formed into very thin sheets used in a variety of packaging.
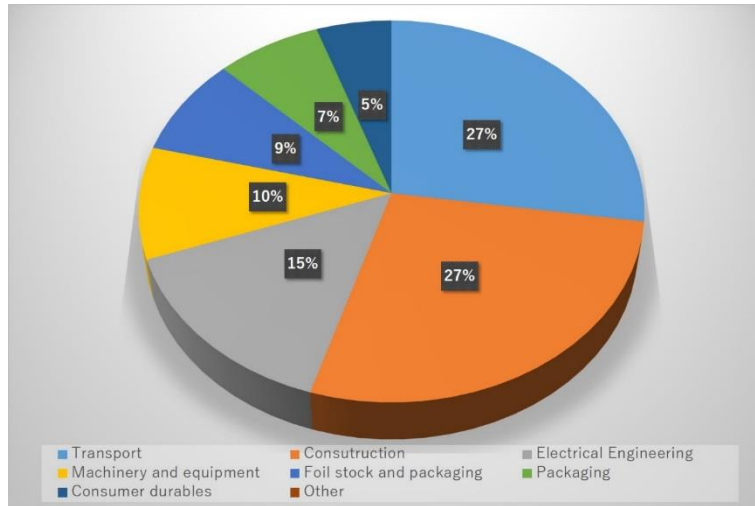
Fig.2 This statistic represents the worldwide demand for semi-finished aluminum products in 2016, with a breakdown by sector [14].

I.3 Conventional production process of aluminum

I.3.1 Primary aluminum production

I.3.1.1 Production of alumina

Industrially, aluminum is produced via two sub-processes: the first known as Bayer process which is the main industrial method to refine bauxite through milling, filtering and cooling to pure alumina [15]. The second sub-process was known as Hall-Héroult and consists of aluminum metal extraction via electrolysis of pure alumina (Al_2O_3) which is dissolved in cryolite $NaF-AlF_3$ solution as shown in Fig. 2. However, this conventional industrial process expresses two main downsides, such as the requirement of high energy consumption and high greenhouse gasses emission (CO_2, CF_4, and C_2F_6).

I.3.1.2 Electrolytic reduction

Primary aluminum is produced by electrolytic reduction of alumina (Al_2O_3) dissolved in a molten bath of main sodium aluminum fluoride (cryolite) at a temperature of approximately 960°C. The electrolytic process occurs in steel cells lined with carbon. Carbon electrodes extend into the cell and serve as anodes whereas the carbon lining of the cell is the cathode. At the cathode level, liquid aluminum is produced, while at the anode, the combination of oxygen and carbon forms carbon dioxide. The overall electrolytic reaction is given as below:

$$\frac{1}{2} Al_2O_3 + \frac{3}{4} C \rightarrow Al + \frac{3}{4} CO_2, \tag{1}$$

To maintain an alumina content of 2-6% in the molten bath, alumina is added to the cells. A modern plant uses computer-controlled additions. To lower the bath melting point, fluoride components are added in a way to assure operation of the cells at a lower temperature. Aluminum fluoride (AlF_3) is also added to neutralize the sodium oxide present as an impurity in the alumina. In modern plants, a significant excess of cryolite is seen due to the presence of high content of AlF_3 in the bath. Consequently, fluoride emissions increase as the excess AlF_3 in the bath is increased as seen in Fig. 3.
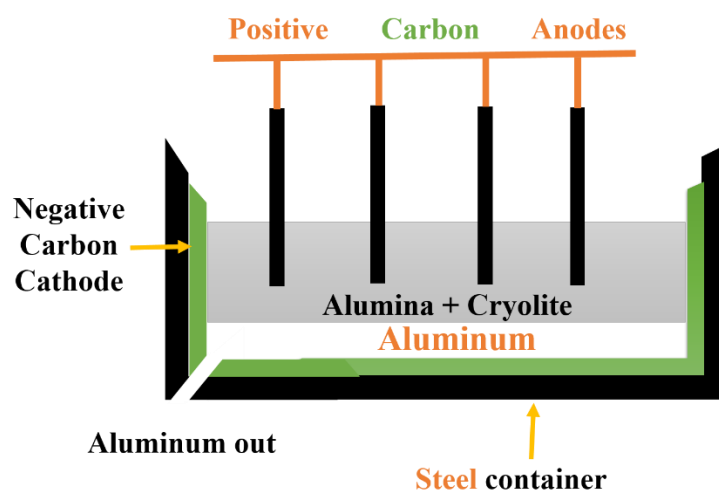
Fig. 3 Hall-Héroult electrolytic smelting cell.

I.3.1.3 Refining Process

After the electrolysis, to remove the impurities such as sodium, calcium oxide particles, and hydrogen, aluminum metals are refined. The refining process consists of injecting a gas into the molten metal in an inline reactor. The choice of the injected gas depends on the impurity type. More information can be found in the Best Available Techniques Reference (BREF) document on non-ferrous metal industries (European Commission, 2001). At this stage at the surface of the molten metal, Skimmings are produced and removed. The secondary aluminum industry will recycle and use these removals.

I.3.1.4 Casting Process

Slabs, T-bars or billets are cast in vertical direct chill casting machines that use water-cooled metal molds and a holding table at the bottom part of the molds. The table is lowered as the ingot is formed. Other casting methods include the use of metal molds (static or continuously moving), continuous casting of thin sheets and continuous casting of wire rod.
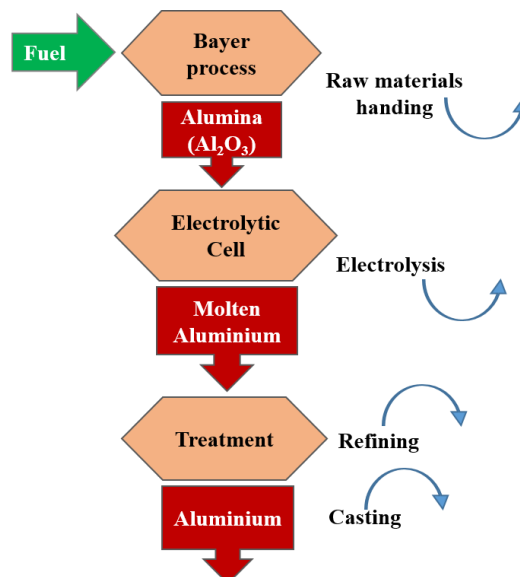
Fig. 4 Schematic process for the primary production of aluminum.

Additional small quantities of skimmings are also produced at this stage and are removed from the surface of the molten metal.

I.4 Passive effect of conventional production methods of aluminum on the environment

Wide-Scale industrial production of aluminum was achieved until the twentieth century due to further efficiencies reached in the Bayer process [16]. Karl Joseph Bayer, an Austrian chemist, first developed and obtained a patent on his process in 1888. The first plant using the Bayer process was opened in 1893. Increasing electrical plant capacities allowed wide-scale industrial aluminum processing to expand rapidly in the twentieth century. The Bayer method of extraction is still in use today as the most common and economical method of isolating alumina, a partially purified form of aluminum [17,18]. Bayer process consists of three stages, extraction, precipitation followed by the calcination of the precipitated product.

The aluminum production process from extraction to processing has a significant impact environmental associated with each stage of the production process. Greenhouse gas emission represents the major environmental impact caused by the refining and smelting processes. The cause of this gases is the electrical consumption of smelters and the byproducts processing. The primary production generated greenhouse gases include PFC (perfluorocarbons), PAH (polycyclic aromatic hydrocarbon), fluoride, SO_2 (sulfur dioxide), and CO_2 (carbon dioxide). Within these generated gases, PFC is produced from the smelting process and are the most potent. In the United States, the primary aluminum production is considered as the leading source of perfluorocarbon emissions. The manufacturing of anodes for smelters electrolytic process is considered to be the source of PAH emissions. Sulfur dioxide and sodium fluoride are generated and emitted from electrical plants and smelters, while SO_2 is considered as one of the primary precursors of acid rain. CO_2 emissions occur during smelting and result from the consumption of carbon anodes and PFC emissions(Fig.5).

In order to track, reduce and report emissions and other environmental impacts

caused by the primary aluminum production, a joined efforts between the US Environmental Protection Agency, the aluminum industry cooperates in the Voluntary Aluminum Industrial Partnership have been built. Recent studies show that this joint effort has made significant progress in PFCs emissions reducing.

In case of mixing occurred between the atmospheric pollutants from primary aluminum production and water vapor can lead to acid rain occurrence. In the case when soil pH remains at or above 5, aluminum poses no danger of environmental toxicity, however, the soil pH is lowered by acid rain and leading aluminum into solution. An aluminum solution can reach into the water supply in where the damages caused can be significant such as creation acidified lakes. Naturally, the amount of aluminum going into the environment far exceeds anthropogenic contributions due to regular weather processes. Distinct advantages can be seen as the results of aluminum recycling process in the life cycle analysis of aluminum. The primary benefit of recycling aluminum is reduced energy consumption. Aluminum recovery from scrap requires only 5 percent of the energy required to extract it. Therefore, secondary aluminum production from recycling scrap has the potential to reduce greenhouse gas emissions significantly. Aluminum cans represent the most common source of aluminum scrap. However, other sources can be considered as viable such as automobiles, building materials, and appliances. Furthermore, the quality of aluminum is not affected by the number of recycling cycles. If exposed to large amounts of aluminum it could be toxic to humans. However, a high exposure is limited to few people with work related to aluminum extraction such as miners or aluminum production workers, and dialysis patients. While there is some evidence linking aluminum to Alzheimer's disease, increased aluminum intake has yet to be a proven cause of the onset of Alzheimer's. Otherwise, aluminum is not significantly bio-accumulated in plants and animals.
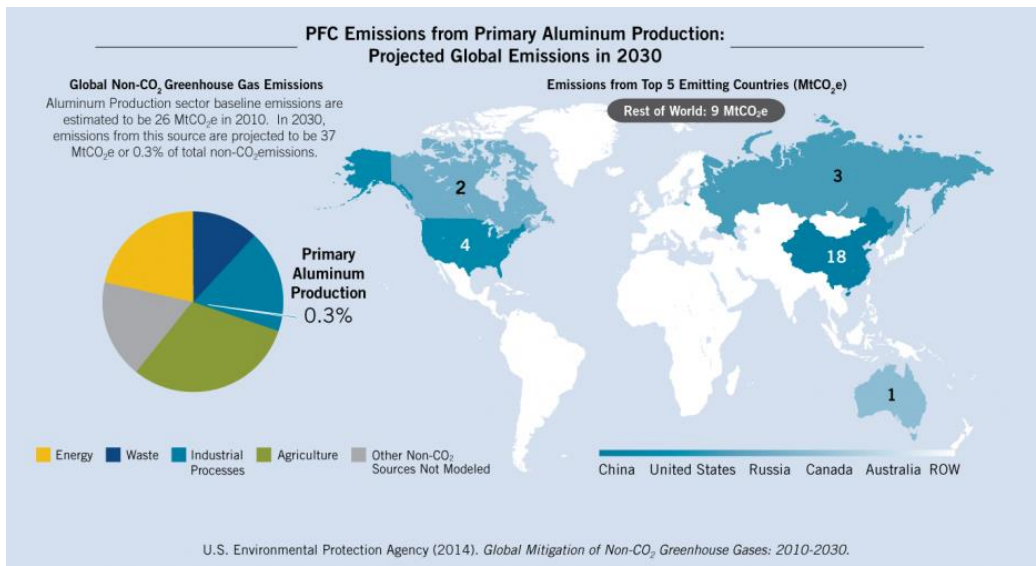
Fig. 5 PFC Emissions from primary Aluminum production projected global Emissions in 2030 [17, 18].

Chapter II. Aluminum reduction, Background, Production Methods and Research Works Objectives

Introduction

Aluminum is the most abandonment materials in the world and is considered to be the most versatile engineering materials across a broad range of applications. To this end, we discuss in this first chapter the worldwide usage and different methods of aluminum. Moreover, we will discuss the current production methods of aluminum while expressing their advantages and inconvenient. Finally, we will discuss the objectives and aims of this research work.

II.1 Survey on carbothermal reduction process

II.1.1 carbothermal reduction of oxides materials

The carbothermal reduction process of oxide materials is known to be an interesting route due to its simplicity, low cost and high purity of produced materials [19].

One of the most critical elements on Earth for life is Carbon. Besides, chemistry has a specific field focused on carbon study, which is the organic chemistry. While carbon can be the leading material in many types of research, it can also be considered as coadjutant actor aiming the research in materials science. Which is the case of carbothermal reduction method, in which the carbon is used to assist in the synthesis process.

The metal oxides undergoing reduction should be less stable than CO according to thermodynamics, while the metal must be a weak carbide-former. An oxide of metals such as Iron, Magnesium, silicon, and aluminum possesses these characteristics and hence are efficiently recovered from their oxides using the carbothermal route. The general carbothermal reduction equation can be written as

$$M_xO_y(s) + yC(s) \rightarrow 7\ xM(s) + yCO(g) \qquad (2)$$

Table 2 Comparaison of different reduction agent of oxides

Reduced By	Process
e-	Hall-Héroult process
C	Carbothermal Reduction
H	Hydrogen Reduction

Existent Industrial Carbothermic Reduction: Iron (Fe), Silicon (Si), there is a possibility to apply the Carbothermic Reduction Process on Al_2O_3

II.1.2 Carbothermal reduction of silica

Carbothermal reduction using an electric furnace still the best economical way to produce solar-grade silicon. The commercialization of this process was since 100 years ago. Silica from gravel and stones and Carbon from charcoal, wood chips, coal, and coke, were used as raw material in the silicon generation process which requires high temperatures and much energy. The by-products of reaction process determine the yielding of the reduction [20].

Silicon can be obtained from the reduction of silica in the presence of carbon at high temperature. At present, silicon (metallurgical grade silicon) is being produced using electric arc furnace based on carbothermal reaction. Fig. 6 shows the schematic comparison between conventional Siemens method of direct reduction of silica to silicon and the main objective of the direct carbothermal reduction of silica.

The direct carbothermal reduction of silica is based on the same principle as the primary metallurgical process to produce metallurgical-grade silicon. Therefore, producing high purity silicon with this method requires enhancing the key elements allowing the production of solar-grade silicon.
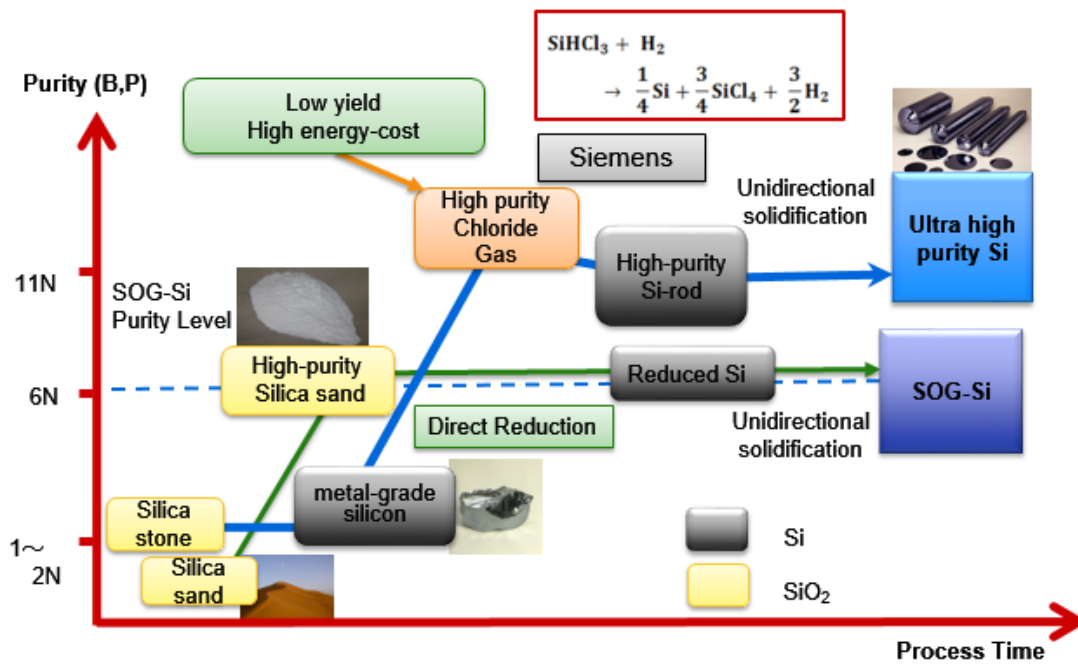
Fig. 6 the schematic comparison between conventional Siemens method of direct reduction of silica to silicon and the primary objective of the direct carbothermal reduction of silica [21].

The direct carbothermal reduction of silica was successfully investigated with our groups, which was integrated and developed the real-time monitoring system of our induction furnace [22]. The silicon reduce was successfully obtained in small-scale graphite crucible by the optimization of the binders in the granulation process [23].

II.2 Direct carbothermal reduction of alumina

II.2.1 process necessary elements

Industrially, aluminum is produced via the Hall-Héroult method in which aluminum metal is extracted by electrolysis of pure alumina (Al_2O_3) dissolved in cryolite NaF-AlF_3 solution. This conventional industrial process, however, expresses two main downsides, such as the requirement of high energy consumption and high greenhouse gases emission (CO_2, CF_4, and C_2F_6) [24-26].

Figure 7 shows the schematic of Hall-Héroult process and carbothermal reduction process. The carbothermal reduction of Al represents one of the potential substitute

methods for metal aluminum production due to its low consumption of electricity and minimal emission of greenhouse gases in comparison with the Hall-Héroult process [27-29]. In the carbothermal process of Al_2O_3, however, the generation of a lot of intermediate products such as aluminum carbide Al_4C_3 and oxy-carbide Al_2OC and Al_4O_4C and volatile aluminum suboxide Al_2O causes quite a low yield of the reduction process from alumina to aluminum [30-32].

Several research groups tried to improve the yield of the carbothermic reduction process via optimization of the experimental process itself. Investigation of the effect of different atmospheric gas (Ar, O_2, and CH_4) during the carbothermic reduction process on the final Al yield was performed [33]. Also, the generation temperature at which each phase of the reduction product appeared (Al_2O gas and solid forms, Al_4O_4C, Al_4C_3) was determined to emphasize the temperature effect on the yield of overall reduction reactions [34]. On the other hand, to investigate the impact of starting raw materials on the yield enhancement, granules of alumina and carbon mixed with sugar powder as a binder were used [35]. While other groups focused on the thermodynamic calculations of the phase diagram which led to studying of by-product behavior during the reduction process in a way to improve the yield. [35-38] However, the improvement of the Al yield by these trials was insufficient for a practical process.

The carbothermal reduction from alumina to aluminum is composed of a series of complicated processes under high-temperature through various intermediate products, such as Al_2O gaseous phase and solid forms Al_4O_4C, Al_4C_3. The complexity of these processes made the thermodynamic explanation and understanding of the different overall reactions behavior during the reduction process difficult. The main reason for the low Al yield in the product is due to the sub-oxide Al_2O gas loss because the Al_2O gas with sublimability is stable only at high temperature and is difficult to control in the furnace. However, the carbothermal reduction of Al_2O_3 is similar to the carbothermal reduction of

silica (SiO_2) concerning the appearance of suboxide gas phase. In the case of silicon (Si), the thermodynamic gaseous phase diagram was utilized to understand the complicated reaction through the SiO gas phase and silicon carbide (SiC) solid phase [39,41].
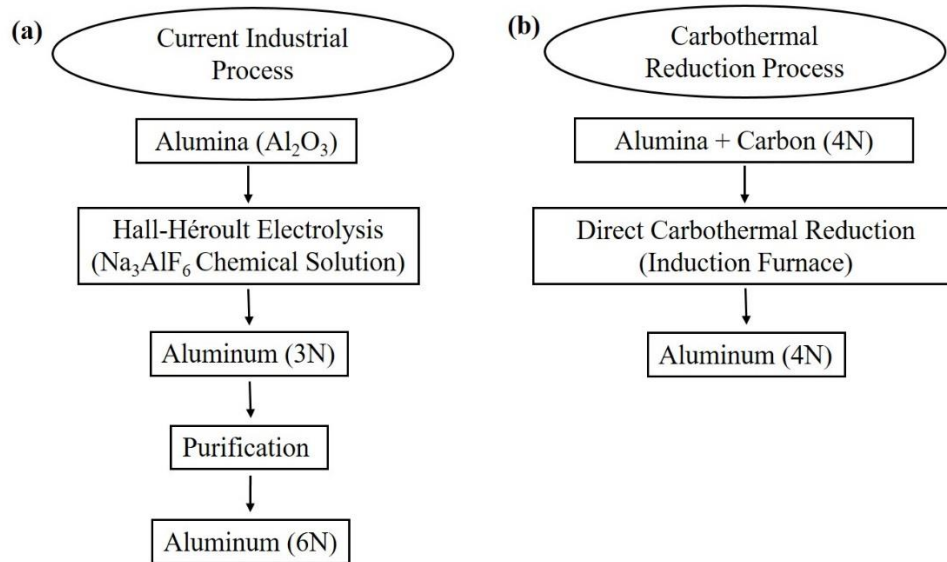
Fig.7 Schematic comparison between current industrial process and carbothermal reduction process of aluminum.

II.2.1 Actual energy, material uses, and environmental impacts in Hall-Héroult and carbothermic reduction process

II.2.1.1 Hall-Héroult

In the Hall–Héroult process, aluminum is produced by the electrolytic reduction of high-grade alumina, which is dissolved in a molten bath consisting mainly of cryolite (Na3AlF6), at a temperature of about 960ºC. The net reaction for the carbon anode Hall–Héroult process is summarized in Equation (3):

$$\frac{1}{2} Al_2O_3 + \frac{3}{4} C \rightarrow Al + \frac{3}{4} CO_2, \tag{3}$$
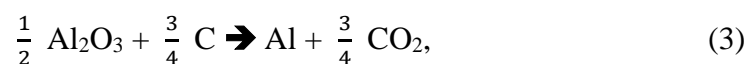
Apply the first law energy conservation principles (assuming no heat losses),

$$E_{in} = \sum_0 (n_o \times h_o) - \sum_i (n_i \times h_i) \tag{4}$$

$$E_{in} = (1 \times 0 + 3\ 4 \times -393.52 - 1\ 2 \times -1675.69 - 3\ 4 \times 0)$$

27

= 542.71 kJ/mole of Al = 20, 100 kJ/kg of Al = 5.59 kWh/kg of Al.

Consumable carbon anodes (0.45 kg for each kg of Al) and a potential of 4.6 V [84] are employed in the electrolytic cell to produce molten aluminum, which is periodically withdrawn from the cathodes by vacuum siphon.

Additionally, another 2.66 MJ=kg Al of fuel energy are spent on carbon anode baking to produce the consumable carbon anodes. As these anodes are made of carbon, they are also in sense a fuel spent in the process. Based on the HHV of coal [85], to produce 1 kg of Al another 15.37 MJ of energy is consumed. In total 3.82 kg of CO_2 equivalent GHG are directly released for each kilogram of aluminum produced; 1.53 kg of CO2 are released from anode consumption, 0.12 kg are released during the anode baking and approximately 2.18 kg of CO2 equivalent of hazardous perfluorocarbons (PFCs) (Commission Decision 2000) are resulted from the process upset known as anode effect[86].

II.2.1.2 carbothermic reduction

Efficient recovery of the aluminum carbide is necessary to make this process economically viable [87]. The net reaction for the carbothermic technology is summarized in Figure 5 and Equation (5).

$$\frac{1}{2} Al_2O_3 + \frac{3}{2} C \rightarrow Al + \frac{3}{2} CO, \qquad (5)$$
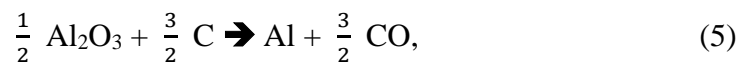
The minimum energy requirement is calculated using Equation (5),

$$E_{in} = (1 \times 0 + 3\ 2 \times -110.53 - 1\ 2 \times -1675.69 - 3\ 2 \times 0)$$

$$= 672.1 \text{ kJ/mole of Al} = 24, 891 \text{ kJ/kg of Al} = 6.92 \text{ kWh/kg of Al}$$

The energy required to change the temperature of aluminum from 298.15 K to 2273.15 K is calculated using Equation; Energy required to change temperature =

$$\int_{T_0}^{T} cp(T)dT \qquad (6)$$

This results in a value of 0.623 kWh/(kg of Al). The energy required for the carbon monoxide temperature change can be calculated in the same manner; this results

in a value of 0.58 kWh/(kg of Al). The total minimum energy requirement is 6.92 +

0.623 + 0.58 = 8.123 kWh/(kg of Al). The theoretical quantities of alumina and carbon

are 1.89 kg/(kg of Al) and 0.67 kg/(kg of Al), respectively (from Equation (3)). The

theoretical carbon monoxide emission is 1.56 kg/(kg of Al) (from Equation (3)).

Table3 summary of Hall-Héroult and carbothermic reduction technologies for 1Kg of Al

Technology	Energy Use(kWh)	Alumina (kg)	Carbon Anode (carbon) (kg)	CO_2(kg)-(CO)(kg)
Hall-Héroult	15.37	1.93	0.45	1.53
carbothermic	10.15	1.89	(0.67)	(1.56)

Table4 summary cost of Hall-Héroult and carbothermic reduction technologies for 1Kg

of Al

Technology	Cost energy	Cost Carbon	Cost alumina
Hall-Héroult	300.02yen	1350yen	1158yen
carbothermic	197.92yen	2010yen	1134yen

$$\frac{\text{Energy use (Carbothermic reduction)}}{\text{Hall}-\text{Héroult}} *100 = \frac{10.15}{15.37} *100 = 66.03\% \quad (7)$$

The carbothermic reduction technology it result in 66.03% energy savings compared

with the current Hall–Héroult technology.

II.2.1.4 Induction heating furnace apparatus

The electric induction furnace is a melting furnace that uses electric currents to melt metal.

Induction heating furnaces are known to be ideal for melting and alloying a wide variety

of metals with minimum melt losses. However, little refining of the metal is possible.

Induction heating is a form of non-contact heating for conductive materials. The principle

of induction heating is mainly based on two well-known physical phenomena:

1. Electromagnetic induction

The principal base of the Induction Furnace is the usage of the electromagnetic induction to heat conductive materials (metals) to its melting point. Three types of induction furnaces depending on the working frequency (50Hz-250kHz):

a. High Frequency

b. Medium Frequency

c. Low Frequency

The capacity of the furnace range from less than 1kg to 100MT, which are used for re-melting of iron & steel (steel scrap), copper, aluminum, precious metals, and alloys. Even most modern foundries use this type of furnaces, and now more iron foundries are replacing Cupolas with Induction Furnace to melt cast iron as the former emit lots of dust & other pollutants. The Steelmaking via Induction Furnace route has certain advantages & disadvantages:

- Advantages of Induction Furnace

1. It has no electrodes and electric arcs which allow productions of steel & alloys low in carbon and occluded gases without any quality problem.

2. Low melting losses & alloying elements.

3. High power efficiency, therefore, cost-effective.

4. Precise control of the operating parameters.

- Disadvantages of Induction Furnace

1. Refining in Induction Furnace is not as intensive or effective as in Electric Arc Furnace (EAF).

2. Life of Refractory lining is low as compared to EAF.

3. Removal of S & P is limited, so the selection of charges with less impurity is required.

A high-frequency induction heating apparatus utilizes the principle of electromagnetic induction as shown in Fig. 8.
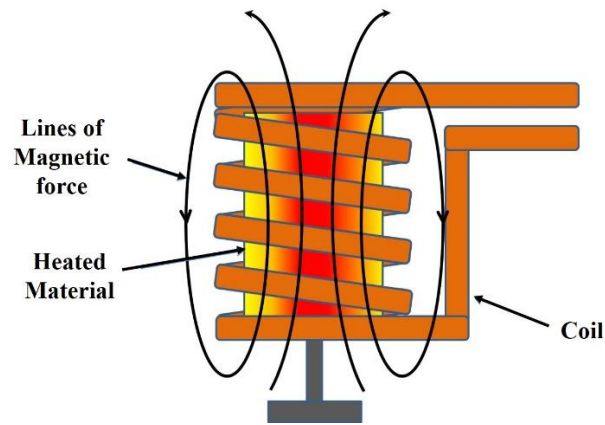
Fig.8 Schematic illustration of the induction heating principle.

Magnetic force lines are generated by applying an alternating current to a coil around the crucible of a heating object, and an eddy current is generated in the heating object by being influenced by magnetic lines of force. The object to be heated is heated by the generation of Joule heat corresponding to the electric resistance depending on the electric resistance of the object to be heated and the applied voltage. A power source with a maximum output of 10 [kW] was used as the source of energy.

II.2.2 Effect of Al₄C₃ on carbothermal reduction of aluminum

The need to produce aluminum without consuming large amount of electrical energy has become apparent in countries, where the cost of electricity is high due mainly to its generation by foreign oil and high capital costs.

Efforts to optimize carbothermal reduction of alumina under heating using Al_4C_3 as an additive. Although, the adding of Al_4C_3 additive to raw material, Al_2O_3 and carbon, was proposed as a way to increase the ratio of partial pressure $P(Al_2O)/P(CO)$. In order to understand the usage of this technique, an attempts to apply it on the carbothermal reduction of alumina in an induction furnace in which each product will be heated in same conditions with different mass of Al_4C_3 to understand the relationship between the raw material input alumina, carbon and Al_4C_3 additive with the final product aluminum and which intermediates species will interfere and would be the cause of the high yield of

carbothermal reduction of alumina using an induction furnace. However, to proceed such experimental procedure, at first, an understanding of the thermodynamic background for the process reactions is necessary and will be explained in the next section in details discussed all the possible relation between the materials existing in the carbothermal reduction of alumina to produce aluminum.

II.2.2.1 Process reactions

The carbothermal reduction process is a versatile method, and it is based on the Ellingham diagram, as presented in Fig.9. The Ellingham diagram of several oxides consists of the plot of Gibbs free energy versus temperature and reactions appears like straight lines due to the following equation:

$$\Delta G = \Delta H - T \Delta S \tag{8}$$

In which: ΔG is the change in the Gibbs free energy, ΔH is the enthalpy of formation, ΔS is the entropy variation, and T is the temperature.
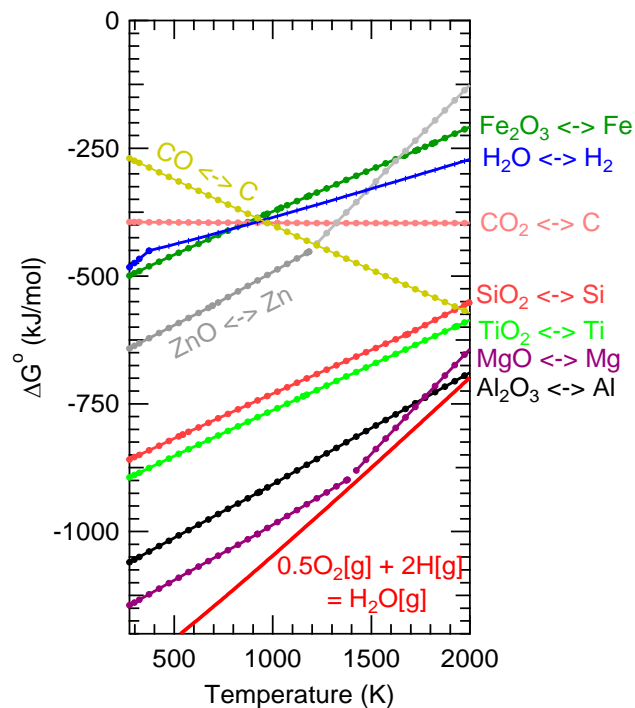
Fig. 9 The Ellingham diagram for several elements. Iron, hydrogen, carbon, silicon, titanium, Magnesium, aluminum and zinc are indicated [42].

The free energy of an element decreases when that element change to oxide, so the ΔG axis presents negative values in Fig. 9. When a reaction is spontaneous, the intercept is related to the enthalpy of formation. The hydrogen reduction line crosses only the iron and zinc curves, while the line of carbon reduction passes through the silicon curve. This indicates that normal hydrogen gas can not reduce alumina, silica or any other oxides without intersection of their two lines. While when using the carbon as a reductant agent the reduction reaction consists of a vast number of complicated reaction paths. The reaction between alumina and carbon materials happens under atmospheric pressure in the range of temperature from 1773K to 2473K (1500 °C to 2200 °C) [43]. Based on the temperature difference, the furnace can be divided into two zones: the low-temperature zone (outer zone) and the high-temperature zone (inner zone). In the inner zone, molten alumina and aluminum carbide react with each other and form Al_2O gas and CO gas according to reactions 9 and 11, for reactions 8 and 10 the Al_4C_3 and Al form, which is the concern of this study.
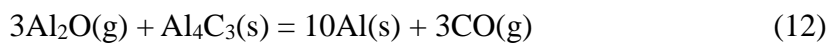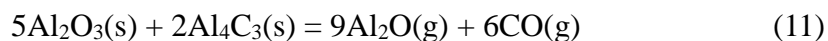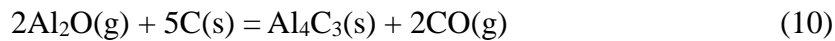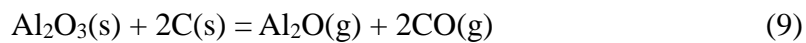
$$Al_2O_3(s) + 2C(s) = Al_2O(g) + 2CO(g) \qquad (9)$$

$$2Al_2O(g) + 5C(s) = Al_4C_3(s) + 2CO(g) \qquad (10)$$

$$5Al_2O_3(s) + 2Al_4C_3(s) = 9Al_2O(g) + 6CO(g) \qquad (11)$$

$$3Al_2O(g) + Al_4C_3(s) = 10Al(s) + 3CO(g) \qquad (12)$$

At first, Al_2O_3 reacts with carbon to generate Al_2O and CO gasses via reaction in Eq. (9). And then, Al_2O gas reacts with carbon to generate Al_4C_3 via reaction in Eq. (10). On the other hand, Al_2O_3 reacts with Al_4C_3 to generate Al_2O and CO gasses via reaction in Eq. (11). Finally, Al_4C_3 will react with Al_2O gas to generate Al metal via reaction in Eq. (12).

II.3 Research Work Objectives

II.3.1 Optimization of heating temperature of carbothermal production process of aluminum in order to achieve higher yield for sensing application

Recently the study of aluminum-based surface plasmon resonance sensors (SPR) for real-time, label-free, and multiplexed detections for chemical and biomedical applications have attracted a considerable attention due to the effective stability of aluminum compared to conventional noble metals such as Ag and Au. Currently, the electrolytic Hall-Héroult process represents the conventional and commercialized process for the production of aluminum from alumina. However, this process suffers from higher cost due to its immense energy requirements, and a number of by-processes implicated to reach the final product. In this paper, to overcome such advantages of the conventional process, the carbothermal reduction process of alumina using an induction heating furnace and carbon as a reductant agent were investigated to determine the optimum heating temperature condition for the achievement of a higher yield of the process. The phase diagram for the aluminum-oxygen-carbon represents quite a valuable asset. Therefore, it was simulated and used to determine theoretically the temperature and gas conditions used for the experimental process. The optimum heating temperature of 1750ºC was determined based on the analyzing of the experimental results based on the comparison of the obtained Al yield for various heating temperature profiles.

II.3.2 Investigation and Optimization of carbide Additive Effect on Enhancement of Carbothermal Production of aluminum from alumina

In terms of electricity consumption, the carbothermic reduction process of alumina (Al_2O_3) represents one of the promising candidates to overcome the current industrial Hall-Héroult process for the production of aluminum (Al) from Al_2O_3. The yield of the carbothermic reduction process of Al_2O_3, however, is not high enough to be considered

as a substitute for the present industrial process. The calculation of the gas phase diagram of Al-O-C system suggests the possibility of the enhancement of the Al product yield by the increase of the ratio of the partial pressure Al_2O/CO. An increase in the ratio of the partial pressure Al_2O/CO can be expected by the reaction of aluminum carbide (Al_4C_3) and Al_2O_3. We investigated the effect of adding Al_4C_3 on the enhancement of the final Al yield in the production process. In the case without Al_4C_3 additive, the Al yield was only 2.33 %, while, in the case of adding Al_4C_3 additive with Al_2O_3: Al_4C_3 = 1:0.05 in molar ratio, the Al yield increased drastically up to 15.86 %.

Chapter III: Experimental Procedure

This chapter is dedicated to explain the experimental details for each experiment procedure related to both research works including the thermodynamic background and the experimental setup starting with the temperature optimization experiment for higher yield of the reduction for sensors applications and followed by the optimization of the oxy-carbide additive on the reduction yield.

III.1 Experimental Procedure #1 "Heating-Temperature Optimization"

Real-time sensing for many applications such as safety of food, medical diagnostic and monitoring of environment represents nowadays a requirement to maintain our daily life tasks [44-46]. Surface plasmon resonance (SPR) sensing is label-free capable sensors to fulfill such tasks due to their simplicity and easy to use, their small detection volume and assurance of multiple detections [47, 48]. However, commercially, the majority of produced SPR sensors are made of noble metals such as Au and Ag due to their low optical losses in visible-infrared range and chemical stability [49]. In the other side, Ag is known for its easy oxidation, which requires the deposition of a passivated dielectric film, which led to a high cost of SPR sensor production based on noble metals [50]. Recently, SPR-based aluminum sensors technology has emerged due to the cost-effectivity and stability of aluminum metal [51-53]. The current industrial production process of Aluminum (Al) is Hall-Héroult process which includes two sub-processes [54,55], starting by the dissolving of Alumina (Al_2O_3) infused Cryolite (NaF-AlF$_3$) [56,57] and followed by electrolysis via direct current and in which Al will be deposited at the bottom of the cell and CO_2 is released [58]. However, this conventional process shows a colossal drawback represented in its second by-process [59-61]. The electrolytic process is known to be a massive energy consuming process [62,63] To overcome such drawback, the direct carbothermal reduction process represents a substitute route for the

production of aluminum from a raw materials mixture of alumina and carbon [64,65]. Although the concept of the carbothermal reduction has been around for at least 50 years, it has long been considered impractical due to the high temperature (2000ºC) and complex reactions during the reduction process [66-69]. Several research groups obtained aluminum via carbothermal reduction of alumina using different types of furnaces such as the Advanced Reactor Process Furnace (ARP) developed in 2011 by Aloca Norway Carbothermic group, and it includes a diverting system for aluminum gas. The ARP furnace is big enough to produce several tons of aluminum. However, it stills a pilot test and is far away from commercialization [70-72]. Other company known as ENEXAL used the carbothermal reduction under vacuum in an enhanced electric arc furnace including a dual condensation zone and modified form of supplied raw materials pellet, however, the process still under experimental research and is far away to see the light as an alternative for electrochemical process [73].

Induction heating furnace has been quite a useful energy source for the carbothermal reduction of silica for production of solar-grade silicon in our group [74]. Comparing aluminum to silicon, both materials requires a higher production temperature. Therefore, we opted for usage of induction heating as an energy source to reduce alumina to aluminum. Despite that the carbothermal reduction is a one-step process, the reactions occurring during the reduction are quite complicated [75]. Although the extensive research concerning the development of an alternative carbothermal process for Hall-Héroult, no promising results have been reached due to several difficulties related to precise understanding of the overall reaction, temperature and heating time during the reduction process. Therefore, the stability phase diagram Al-O-C for the different element existing during the reduction process is essential to understand the behavior and direction of the solid, liquid and gas phases of the reduction materials [76]. Aluminum materials are produced around 2100ºC which represents quite a high temperature requiring the

consumption of higher electric sources for the necessary heating period [77]. The lack of experimental background defining the optimum temperature and heating time represents a significant problem in order to enhance the carbothermal reduction process of alumina [78]. In this first part of the experimental chapter, the Al-O-C phase diagram was simulated and used for understanding theoretically the overall reaction during the reduction of alumina, and based on the discussed theory; the reduction process heating-temperature was investigated and optimized following the highest amount of alumina recovered in the product in the mean of a higher reduction yield.

III.1.1 Thermodynamic of Al-C-O Phase Diagram

Under the carbothermal reduction process of alumina to produce aluminum, a higher number of overall reactions required to achieve the reduction. In recent years, the usage and enhancement of this process became the object of several studies of research groups. Such as the calculation of the different interaction between the existent sub-products during the reduction process [79], and the investigation of the phase-change occurring during the reduction [80]. While other research groups focused on the optimization of the critical parameter such as the ratio of raw materials, reduction atmosphere (Ar, H_2, and He) and the heating temperature to improve the process yield [81,82]. However, until now, a lack of precise results defining the map for the optimization of the heating-temperature process represents a significant concern for the improvement of the process yield. A simplified route containing three equations chosen as overall reactions to reach the final product are illustrated bellow (13-15). Al-O-C phase diagram was calculated and simulated based on the three reactions above with data taken from MALT2 [83]. The relationship between the reacted raw materials (Al_2O_3 and C), the by-products in their solid form Aluminum oxy-carbide (Al_4C_3) and gaseous forms (Al_2O and CO), and the final product (Al). The diagram exhibits the partial pressure ratio of the gaseous forms Al_2O/CO in function of the temperature as shown in Fig. 10. The standard Gibbs energy

of each reaction and its dependency on the required threshold starting temperature, it's shown above under each reaction in a way to express the importance of the threshold temperature definition thermodynamically via the phase diagram.

$$Al_2O_3(s)+2C(s)= Al_2O(g)+2CO(g) \tag{13}$$
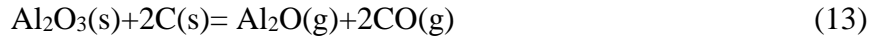
$$\Delta G^0 = 1261-0.536T(kJ) \quad T\geq1773.5K \ (1500ºC)$$

$$2Al_2O(g)+5C(s) = Al_4C_3(s)+2CO(g) \tag{14}$$
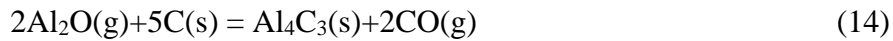
$$\Delta G^0 = -124+0.016T(kJ) \quad T\geq1973K \ (1700ºC)$$

$$3Al_2O(g)+Al_4C_3(s) = 10Al(s)+3CO(g) \tag{15}$$

$$\Delta G^0 = 507.8-0.234T(kJ) \quad T\geq2173K \ (1900ºC)$$

As mentioned the phase diagram of Al-O-C in Fig. 10, is divided to three zones, Zone (I) where the raw materials including the mixture of Al_2O_3 and C start to react at a temperature of 1500ºC (1773.5K) to produce Al_2O and CO gasses through reaction in equation (13). Moving from Zone (I) to Zone (II), Al_2O generation from the zone (I) will increase by an increase of reaction temperature and will react with C in its solid form from Zone (I) to generate Al_4C_3 in its solid-liquid form and CO gas at 1700ºC (1973K) via reaction in equation (14). When reaching a higher partial pressure ratio between $P(Al_2O)/P(CO)$ and sufficient temperature of 1900 ºC (2173K), reaction in equation (15) will start for moving from Zone (II) to Zone (III) which will Lead to production of Al solid-liquid form via interaction between produced Al_4C_3 in Zone (II) and remained generating Al_2O gas from Zone (I).
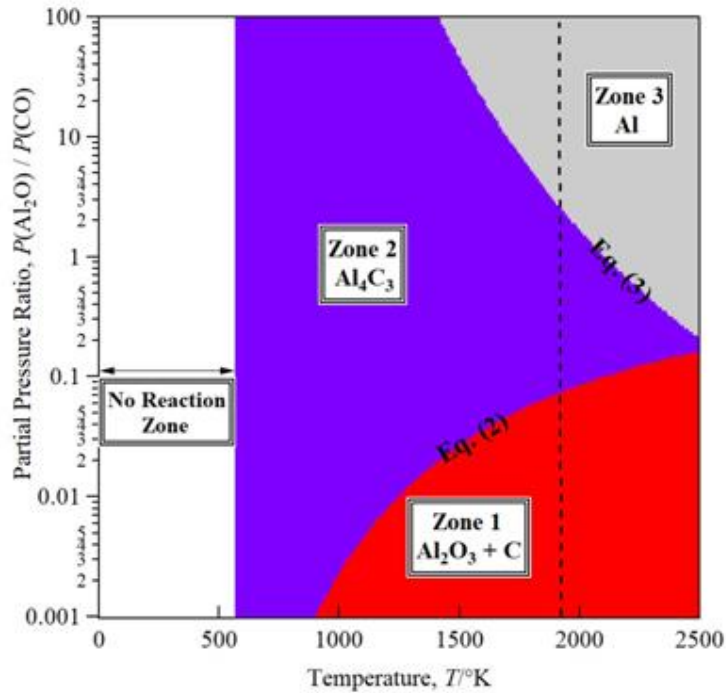
Fig. 10 Al-O-C Phase diagram for the partial pressure ratio of gaseous species Al$_2$O/CO. This diagram shows the variation of the partial pressure ratio Al$_2$O/CO and temperature impact on the reduction of alumina to aluminum based on calculated data from MALT2.

The phase diagram discussion shows that the control of the produced Al yield depends on the partial pressure ratio (Al$_2$O/CO) and reaction's temperature. As a partial conclusion of the thermodynamic discussion, the control and optimization of two key parameters can lead to increase of the reduction process yield. In the next experimental part, the optimization of the heating temperature and its impact on the improvement of the final produced Al yield will experiment and the results discussed in details.

III.1.2. Experimental Setup

Figure 11 shows an illustration of the heated crucible via the induction furnace;
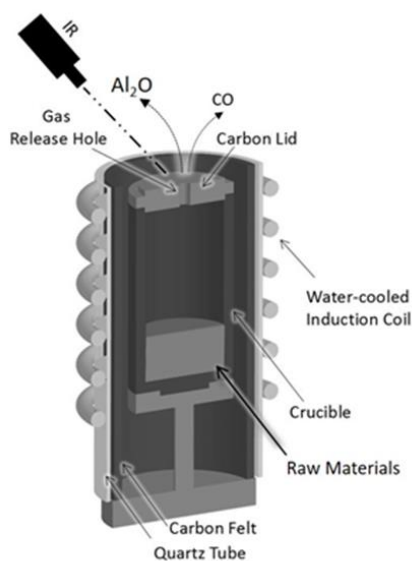
Fig. 11 Schematic figure of the crucible configuration during the reduction process. The crucible was covered with carbon felt and surrounded by a quartz tube as insulation. The crucible temperature measured from the crucible top via an infrared thermometer.

The crucible is made of a high-purity graphite material with an inner diameter of 40 mm and a height of 70 mm. The induction heating furnace generates a power of 30kW (Toei Scientific Industrial CO, Ltd) containing a power supply and a vacuum chamber connected with a quadrupole mass spectrometry (Q-mass) to analyze the gas species generated during the reduction process.

Six mixtures of alumina (diameter 20~100 um, Taiheiyo Cement Corporation Japan) and glassy carbon (diameter 20 um, Tokai Carbon Ltd), were prepared with same molar ratio of raw materials (Al_2O_3:C) = (1:2) and heated with different heating patterns to achieve a heating-temperature comparison between the six samples starting from 1350ºC with sample 1 with a 100ºC increasing step to finally reach sample 6 with a temperature of 1850º as shown in Table 5. The prepared raw material mixtures are shown in Table 6 in which the mass balance of the six experiments is illustrated. The six samples were

installed in the graphite crucible, and it was placed at the center of the induction furnace heating coil. While as a protection of the crucible surrounding, it was covered with a thin layer of carbon felt and inserted into a quartz tube as insulation.

Table 5 Experimental design of six heating-temperature profiles corresponding to each experimental sample.

Sample number	(1)	(2)	(3)	(4)	(5)	(6)
Heating-Temperature (ºC)	1350	1450	1550	1650	1750	1850

Moreover, as shown in Fig. 11, the crucible temperatures were monitored by a high-sensitive single color-type infrared thermometer with a temperature detection range from 651ºC ~ 3500ºC, and it was measured at the top of the crucible (Cap) in each heating experiment. While the vacuum state of the chamber was achieved via a combination of a primary vacuum with a rotary pump and a secondary state vacuum assured with a diffusion pump. We carried out our experiments under argon gas atmosphere which is known to require a higher temperature to achieve the reduction process compare to other reaction atmosphere gasses such as He and N_2. The argon supplied pressure was around 0.07 MPa, and its purpose is to avoid the leakage to outside the vacuum chamber of the lethal to health carbon monoxide gas. A secondary vacuum level of the chamber was achieved as mentioned above, to reach a precise detection of the overall gasses during the reduction process via Q-mass which is essential in this case for the detection of two gasses forms Al_2O and CO. While Al_2O cannot be detected via Q-mass due to its volatility under a specific temperature, CO can be detected. However, it requires a high vacuum to not override the position of N_2 at $(m/Z) = 28$.

Table 6 Mass balance comparison between the six heating-temperatures samples shows that the highest yield of Al obtained in the reduction process corresponding to a heating temperature profile of 1750 ℃ and measured at the cap of the crucible with an estimated error of ±200 ℃ with inside crucible temperature. In order to facilitate the calculation, other oxy-carbide materials appearing in the XRD analysis were gathered in Al_4C_3.

	(1)		(2)		(3)		(4)		(5)		(6)	
	(g)	(Al mol)	(g)	(Al mol)	(g)	(Al mol)	(g)	(Al mol)	(g)	(Al mol)	(g)	(Al mol)
Al_2O_3	5.15	0.10	5.15	0.10	5.15	0.10	5.15	0.10	5.15	0.10	5.15	0.10
C	1.83		1.83		1.83		1.83		1.83		1.83	
Total Input	6.98	0.10	6.98	0.10	6.98	0.10	6.98	0.10	6.98	0.10	6.98	0.10
Total Product	6.69	0.10	6.51	0.10	4.65	0.10	0.74	0.03	1.08	0.03	0.55	0.02
Al_2O_3	4.75	0.09	3.35	0.07	2.61	0.05	0.00	0.00	0.00	0.00	0.00	0.00
C	1.59		2.08		0.13		0.00		0.41		0.00	
Al	0.00	0.00	0.00	0.00	0.00	0.00	0.16	0.01	0.50	0.02	0.19	0.01
Al_4C_3	0.36	0.01	1.08	0.03	1.91	0.05	0.57	0.02	0.17	0.01	0.36	0.01
Lost Gas	0.28	0.00	0.47	0.00	2.33	0.00	6.24	0.07	5.90	0.07	6.43	0.08
Al_2O	0.00	0.00	0.00	0.00	0.00	0.00	2.45	0.07	2.45	0.07	2.80	0.08
CO	0.28		0.47		2.33		3.79		3.45		3.63	
Total Output	6.98	0.10	6.98	0.10	6.98	0.10	6.98	0.10	6.98	0.10	6.98	0.10
Al Yield (%)		0.00		0.00		0.00		6.01		18.35		6.97

III.2 Experimental Procedure #2 "carbide additive optimization"

Aluminum metal is indispensable with various structural materials in automotive and aviation industries [22]. Industrially, aluminum is produced via the Hall-Héroult method in which aluminum metal is extracted by electrolysis of pure alumina (Al_2O_3) dissolved in cryolite $NaF-AlF_3$ solution. This conventional industrial process, however, expresses two main downsides, such as the requirement of high energy consumption and high greenhouse gases emission (CO_2, CF_4, and C_2F_6) [23-25].

Figure 12 shows the flow charts for Hall-Héroult process and carbothermic reduction process. The carbothermic reduction of Al represents one of the potential substitute methods for metal aluminum production due to its low consumption of electricity and minimal emission of greenhouse gases in comparison with the Hall-Héroult process [26-

28]. In the carbothermic process of Al_2O_3, however, the generation of a lot of intermediate products such as aluminum

carbide Al_4C_3 and oxy-carbide Al_2OC and Al_4O_4C and volatile aluminum suboxide Al_2O causes quite a low yield of the reduction process from alumina to aluminum [29-31].
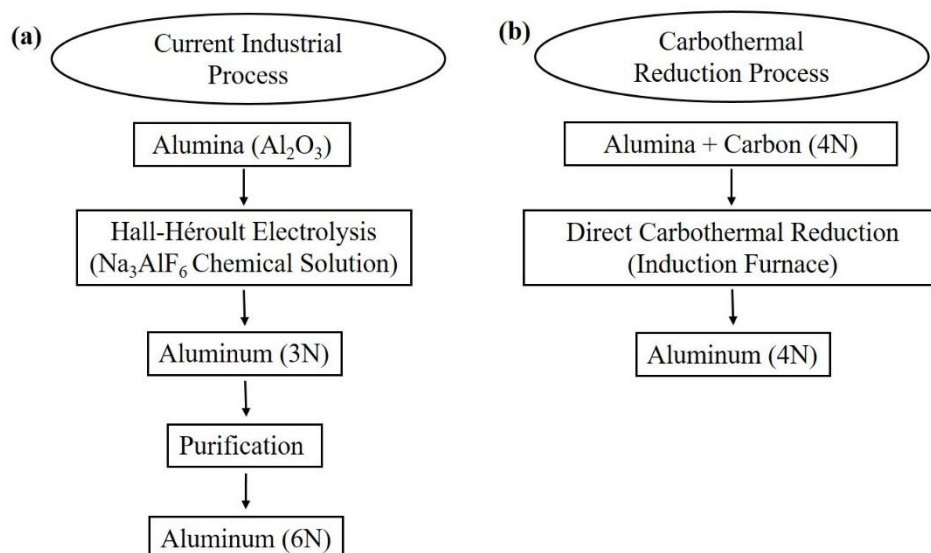
Fig. 12 schematic comparison between current industrial process and carbothermic reduction process for the production of aluminum: (a) Hall-Héroult Electrolytic process and (b) our optimized carbothermic reduction process.

Several research groups tried to improve the yield of the carbothermic reduction process via optimization of the experimental process itself.   Investigation of the effect of different atmospheric gas (Ar, O_2, and CH_4) during the carbothermic reduction process on the final Al yield was performed [32]. Also, the generation temperature at which each phase of the reduction product appeared (Al_2O gas and solid forms, Al_4O_4C, Al_4C_3) was determined to emphasize the temperature effect on the yield of overall reduction reactions [33]. On the other hand, to investigate the impact of starting raw materials on the yield enhancement, granules of alumina and carbon mixed with sugar powder as a binder were used [34]. While other groups focused on the thermodynamic calculations of the phase diagram which led to studying of by-product behavior during the reduction process in a

way to improve the yield [35,36]. However, the improvement of the Al yield by these trials was insufficient for a practical process.

The carbothermic reduction from alumina to aluminum is composed of a series of complicated processes under high-temperature through various intermediate products, such as Al_2O gaseous phase and solid forms Al_4O_4C, Al_4C_3. The complexity of these processes made the thermodynamic explanation and understanding of the different overall reactions behavior during the reduction process difficult. The main reason for the low Al yield in the product is due to the suboxide Al_2O gas loss because the Al_2O gas with sublimability is stable only at high temperature and is difficult to control in the furnace. However, the carbothermic reduction of Al_2O_3 is similar to the carbothermic reduction of silica (SiO_2) concerning the appearance of suboxide gas phase. In the case of silicon (Si), the thermodynamic gaseous phase diagram was utilized to understand the complicated reaction through the SiO gas phase and silicon carbide (SiC) solid phase [37].

In this research work, we calculated the thermodynamic phase diagram with the partial pressure ratio of Al_2O and CO ($P(Al_2O)/P(CO)$). This diagram suggests the possibility of enhancement of Al yield by the increase of $P(Al_2O)/P(CO)$, which can be increased by the additive of Al_4C_3. We performed the optimization of Al_4C_3 additive under carbothermic reduction of Al_2O_3. At the optimal condition, the Al yield was improved 15 times as large as that without Al_4C_3.

III.2.1 thermodynamic of Al-C-O Phase Stability Diagram

The carbothermic reaction from Al_2O_3 to Al are described as following equations:

$$Al_2O_3(s) + 2C(s) = Al_2O(g) + 2CO(g) \tag{9}$$

$$2Al_2O(g) + 5C(s) = Al_4C_3(s) + 2CO(g) \tag{10}$$

$$5Al_2O_3(s) + 2Al_4C_3(s) = 9Al_2O(g) + 6CO(g) \tag{11}$$

$$3Al_2O(g) + Al_4C_3(s) = 10Al(s) + 3CO(g) \tag{12}$$
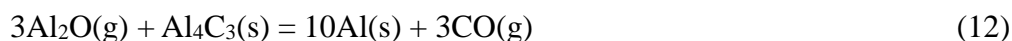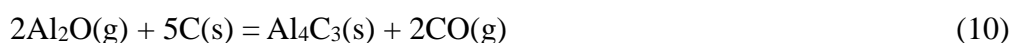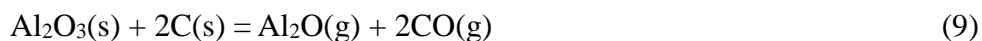
Where (g) and (s) indicate the gas and solid phases, respectively. At first, Al_2O_3 reacts with carbon to generate Al_2O and CO gasses via reaction in Eq. (9). And then, Al_2O gas reacts with carbon to generate Al_4C_3 via reaction in Eq. (10). On the other hand, Al_2O_3 reacts with Al_4C_3 to generate Al_2O and CO gasses via reaction in Eq. (11). Finally, Al_4C_3 will react with Al_2O gas to generate Al metal via reaction in Eq. (2). Only the reactions in Eqs. (9)(11) can generate the Al_2O gas. The ratio of partial pressure $P(Al_2O)/P(CO)$ corresponding to the reaction in Eqs. (10) and (12) are expressed in Table 7.

Table 7 comparison of the mol ratio between Al_2O and CO gasses generated from the reaction in Eqs. (9) and (11). In the case of reductant Al_4C_3, the ratio expresses a high ability to generate amount of Al_2O gas based on amount of CO gas.

	P_a	P_b
Reductant to Al_2O_3	C	Al_4C_3
Reaction Eq. No	(1)	(3)
Mol. ratio (Al_2O/CO)	0.5	1.5

In Eqs. (10) and (12), the sum of coefficients for the gas phases (Al_2O and CO) on the reactant side equals to that on the product side. Under this restriction, two gas phases $P(Al_2O)$ and $P(CO)$ can be described by the ratio of partial pressures $P(Al_2O)$ and $P(CO)$ on the phase diagram, which is independent of the total pressure $P(Al_2O) + P(CO)$. Fig. 13 shows the gaseous phase diagram for the reactions in Eqs. (10) and (12), which were calculated with the standard Gibbs energy taken from MALT2 [83].
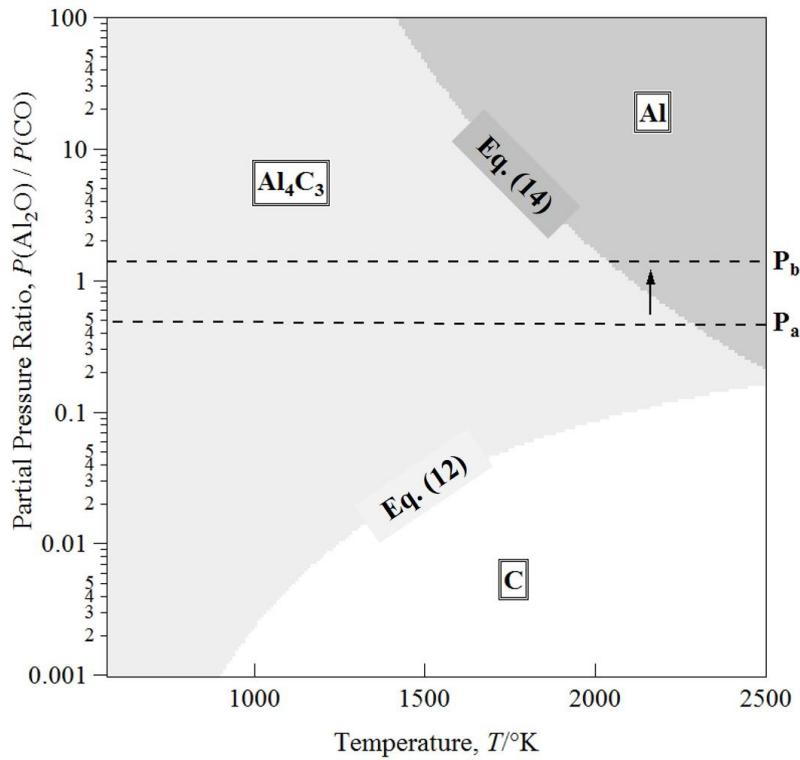
Fig. 13 thermodynamic calculation of phase stability diagram of Al_2O/CO gas phases for reactions in Eq. (9) and in Eq. (11), calculated with data from MALT2. P_a and P_b correspond to the partial pressure ratio $P(Al_2O)/P(CO)$ as shown in Table 5.

The horizontal dashed lines marked as P_a and P_b in Fig. 13 indicate partial pressure ratio as shown in Table 5. The phase diagram suggests that a larger ratio of partial pressures $P(Al_2O)$ and $P(CO)$ can generate Al metal at a lower temperature. Therefore, Al_4C_3 as an additive to raw materials will be expected to accelerate the Al generation.

III.2.2. Experimental Setup

The Al_2O_3 powder (diameter 1 μm, Kojundo Chemical Laboratory, Ltd) and glassy carbon powder (diameter 20 μm Tokai Carbon, Ltd) with a stoichiometric ratio of (Al_2O_3:C = 1:2 in molar ratio) were mixed as a base raw material. Then, Al_4C_3 additive powder was added in the range of 9 various molar ratios, from 0 to 0.1 molar ratio with a step of 0.01 of the starting raw material molar ratio. The mixtures were loaded to a high purity graphite crucible with an inner diameter of 40 mm and height of 70 mm covered with carbon felt and surrounded by quartz tube as an insulator and was installed in the center of the induction furnace as shown in Fig. 14.
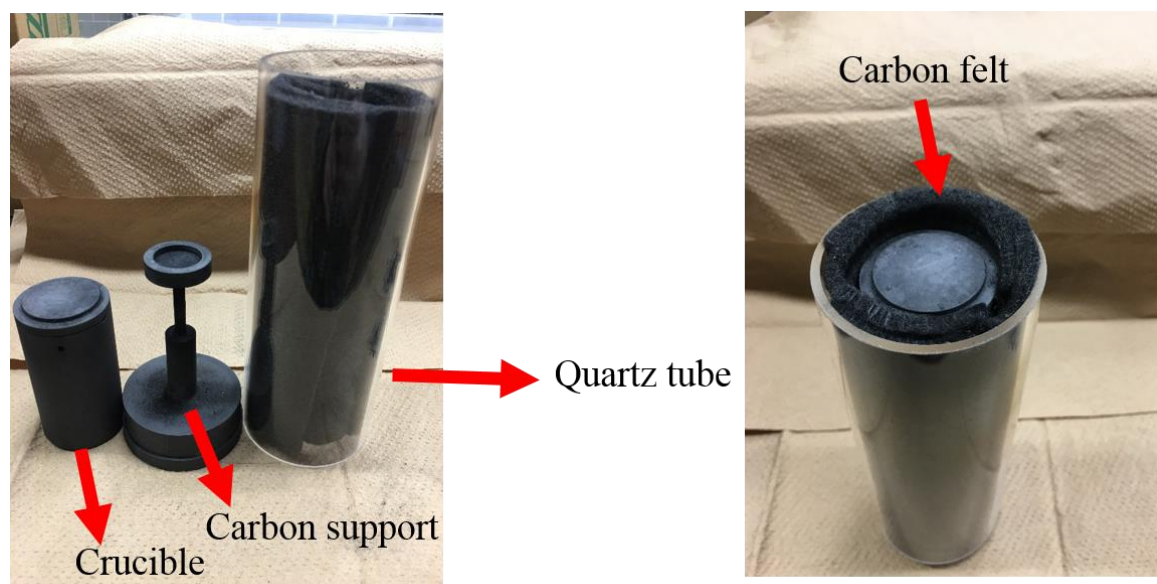
Fig. 14 Real figure of the experimental apparatus. The carbon crucible was surrounded by thermal insulator (carbon felt) and quartz tube as electrical insulation.

The Induction heating furnace is equipped with a highly sensitive color type infrared thermometer (IR-CAQ, CHINO Corporation, Japan) for continuous monitoring of the crucible temperature during the reduction process.

The atmosphere of the furnace was filled with Argon gas with a pressure of 0.09 MPa. All the samples were treated with the same temperature profile as shown in Fig. 15. The furnace was connected to the vacuum chamber with a quadrupole mass spectrometer through the small pin hole to convert the proper pressure. The base gas Ar was used to be a reference to estimate the partial pressure of CO gas.
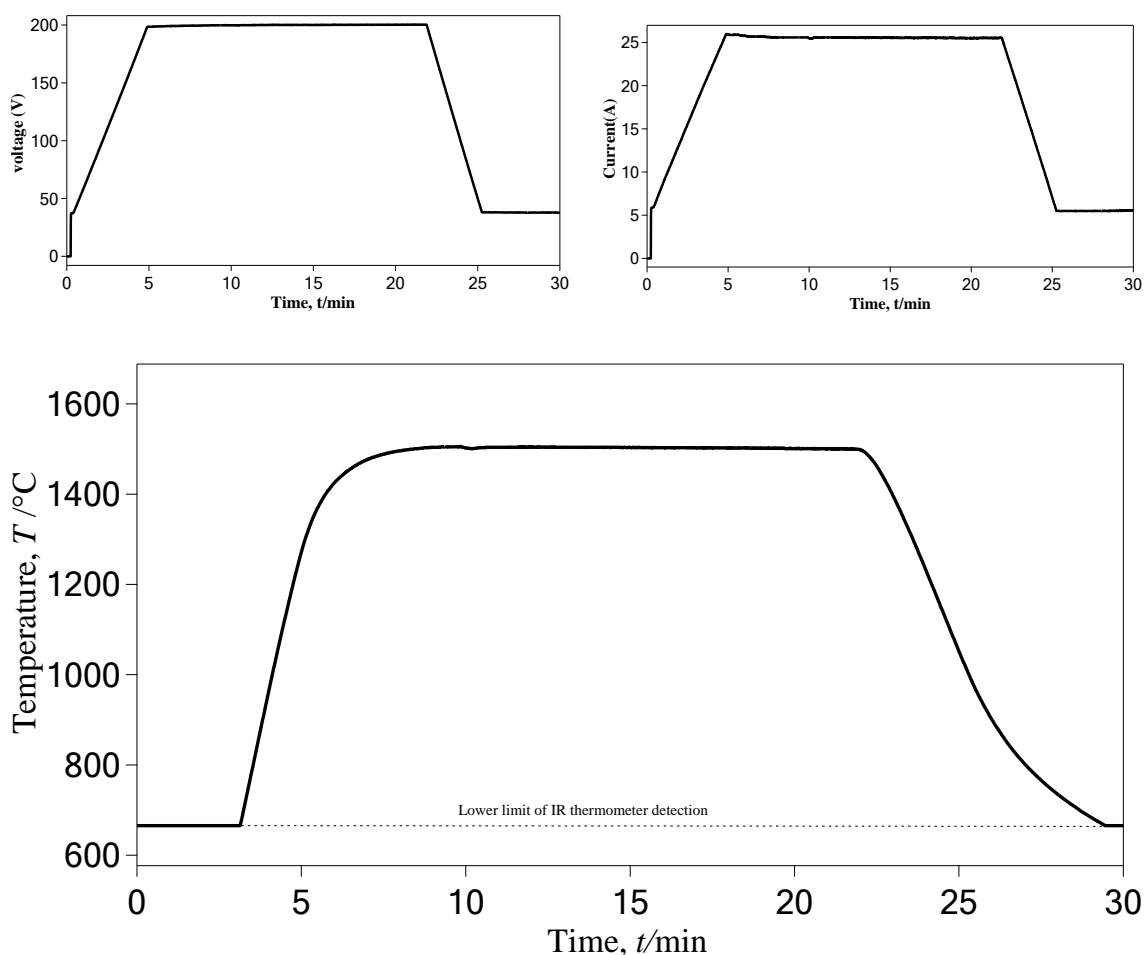
Fig. 15 typical temperature profile measured by the infrared thermometer during the reduction process. The lower limit of the infrared thermometer detection cannot measure the temperature below 665℃.

III.3 Analysis Methods

III.3.1 Quadrupole mass spectrometry (Q-mass)

A quadrupole mass spectrometer analyzed the chamber gas. The induction coil heated the crucible with a frequency of 30 kHz under an open loop control, and a quartz tube was placed in between the crucible and the coil to protect the crucible. The gaseous phases are only Al_2O and CO gasses. The Q-mass spectrometer can only detect CO gas due to mass spectrometry analysis in this study was carried out at room temperature which is an impossible condition to detect the Al_2O gas phase because of its low stability over- Below
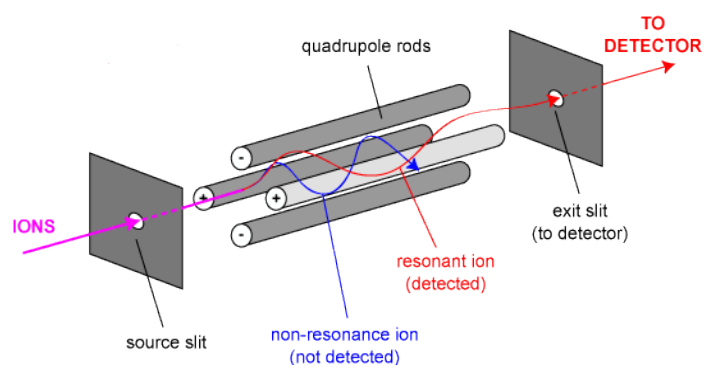
Fig. 16 Functioning Principle of quadrupole mass spectrometry.

1200 ℃ (1473K). The gaseous phase of Al_2O cannot reach the mass analyzer Q because the mass analyzer Q and the chamber are connected by a long metal tube (inside diameter 0.711 mm) with an orifice. The atmosphere during the heating process was pure argon gas (99.999%) with a pressure of 0.07 MPa to avoid leakage of the lethal carbon monoxide gas. The evacuation of the chamber to a higher vacuum order is necessary before the argon gas is deposited because the mass peaks between nitrogen and carbon monoxide overlap completely. The total pressure inside the chamber was recorded manually from the Bourdon gauge connected to the chamber. Depending on the type of technology used, there are a variety of different mass spectrometer systems. Quadrupole

mass spectrometers are today the most widely used devices because they perform well and are distinguished by their compact and robust construction. For mass differentiation, an alternating high-frequency electric field is used for quadrupole devices. A Faraday detector and a secondary electronic multiplier (MES) are used as detectors as shown in Fig. 16.

Quadrupole mass spectrometers allow rapid measurements in milliseconds and have a high dynamic range from ppm to percent. Depending on the intended use in the on-line analysis, these systems can be configured differently and thus provide a favorable price/quality ratio.

III.3.2 Data Key Logger

A data logger recorded the voltage and current of the induction coil, the temperatures of the top of the crucible and the weight variation of the crucible as shown in Fig. 17.
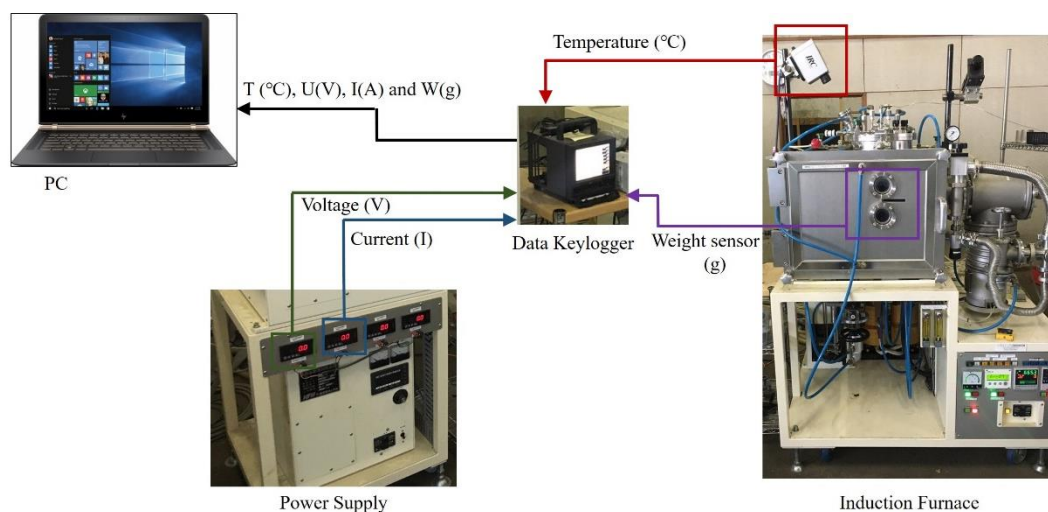
Fig. 17 Schematic illustration of the Data Keylogger operation principle.

III.3.3 X-ray Diffraction (XRD)

III.3.3.1 Ball milling

The Micro Planetary Micro PULVERISETTE 7 is intended for the uniform and extremely fine fragmentation of very small samples of hard to soft, dry or suspended

material up to colloidal fineness. For perfect mixing and homogenization of emulsions or pastes. Maximum sample quantity: 40 ml (Fig. 18) Fields of application Chemistry, biology, pharmacology and pharmaceutical research, medicine, nuclear research, spectroscopy, X-ray fluorescence. The grinding sample is crushed by high energy impacts of the grinding balls (ZrO) and friction between the balls and the grinding bowl wall. In this experiment, the material to be ground at time of 1 minute and 30s. As the shell rotates, the speed ball was 600rpm.

Fig. 18 Real image of the Planetary Micro Mill Pulverisette 7.

III.3.3.2 Regaku SmartLab XRD

XRD (X-ray Diffraction) is a crystal structure analysis utilizing the fact that diffraction phenomenon occurs in a crystal lattice when X-rays are incident on the crystal structure to be measured and strong X-rays are observed in a specific direction. Since each substance has a crystal structure peculiar to each, it is possible to discriminate what the

object to be measured is by examining the crystal peak at the position where the X-ray intensity due to X-ray diffraction phenomemon is high.

In addition, when the sample is a mixture of several substances, the crystal peaks are obtained by superimposing the diffraction peaks of the individual constituent materials, so that it is possible to know the constitution of the sample by detecting and separating them. Further, by comparing the diffraction intensity of each component, the mixing ratio of the sample can be known and quantitative analysis is possible

Fig. 19 Real image of the DRX SmartLab, Rigaku Corporation.

III.3.3.3 XRD Quantitative Analysis

The phase of the product was analyzed using an *x*-ray diffraction system (SmartLab, Rigaku Corporation as shown in Fig. 19) with Cu-*Kα* (λ=1.5405Å) radiation source in the range of 20°≤2θ≤140° with a scan rate of 10º/minute using a 1D silicon strip detector (D/teX Ultra 250). To achieve precise quantification of the material in the product, Si powder was added as a reference to calculate the ratio of Al in products based on the internal standard method using the following equation:

$$I_{(hkl)\alpha} / I_{(hkl)\beta} = q (X_\alpha / X_\beta) \qquad (16)$$

where $I_{(hkl)\alpha}$ and $I_{(hkl)\beta}$ are the peak intensities of the sample and the Si standard, respectively. X_α and X_β are the weight fractions of the sample and the Si standard, respectively. The calibration constant q is estimated from the ratio of the *x*-ray peak intensities of $I_{(hkl)\alpha} / I_{(hkl)\beta}$ as a function of $(X_\alpha / X_\beta .)$, was 1.0682 for Al (200) based on Si (311). This calibration was used for quantification of Al_4O_4C, Al_4C_3, Al, Al_2O_3, and C in the product as showing in Fig.20

the method is used in which a standard internal substance having a constant weight ratio is mixed with a sample and the ratio between the diffraction line intensity I_s according to this internal standard and the diffraction line intensity I_1 of the component to be determined is taken.
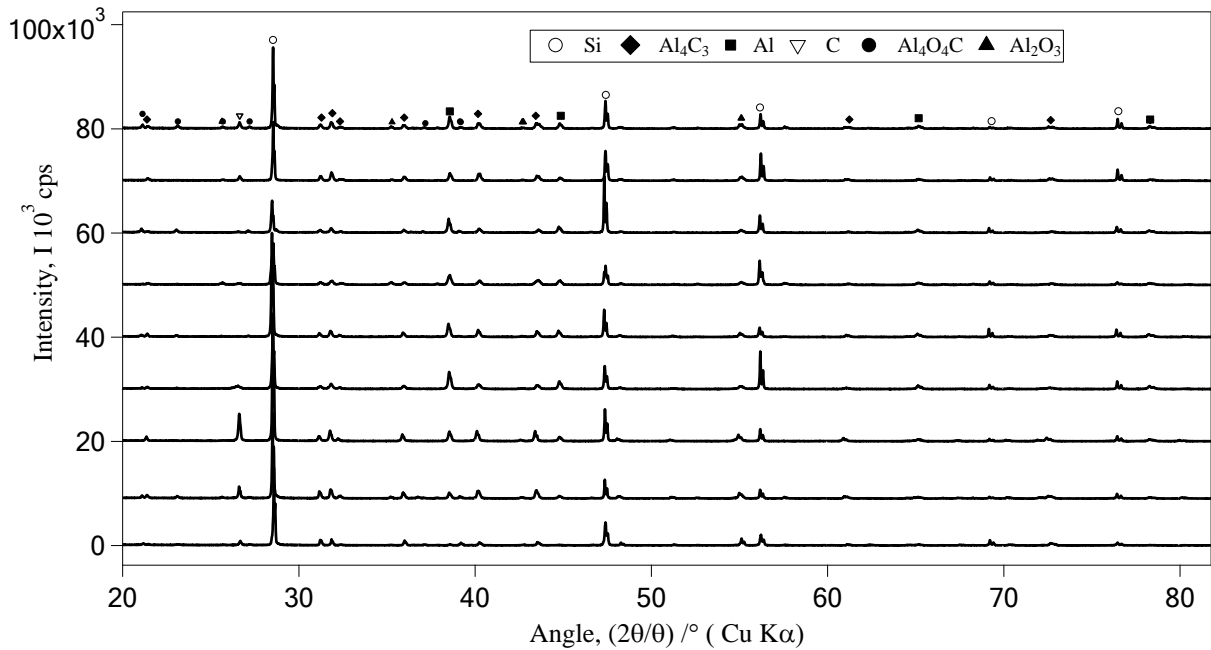
Fig. 20 X-ray diffraction patterns of obtained products using silicon for internal

standard calibration.

In the internal standard method, the mass ratio M_1 of the desired component and the calibration curve of I_1 / I_s are prepared. To create a calibration curve, first, prepare several samples with different mixing ratios of ingredients and add a constant weight ratio of internal standard to each sample. By measuring the diffraction line intensities I_1 and I_s of the sample and drawing a calibration curve of I_1 / I_s: M_1, it becomes a straight line passing through the origin. Therefore, I_1 / I_s of an unknown sample is measured and compared with the calibration curve of I_1 / I_s: M_1 prepared beforehand, the mass ratio M_1 to be obtained is immediately obtained.
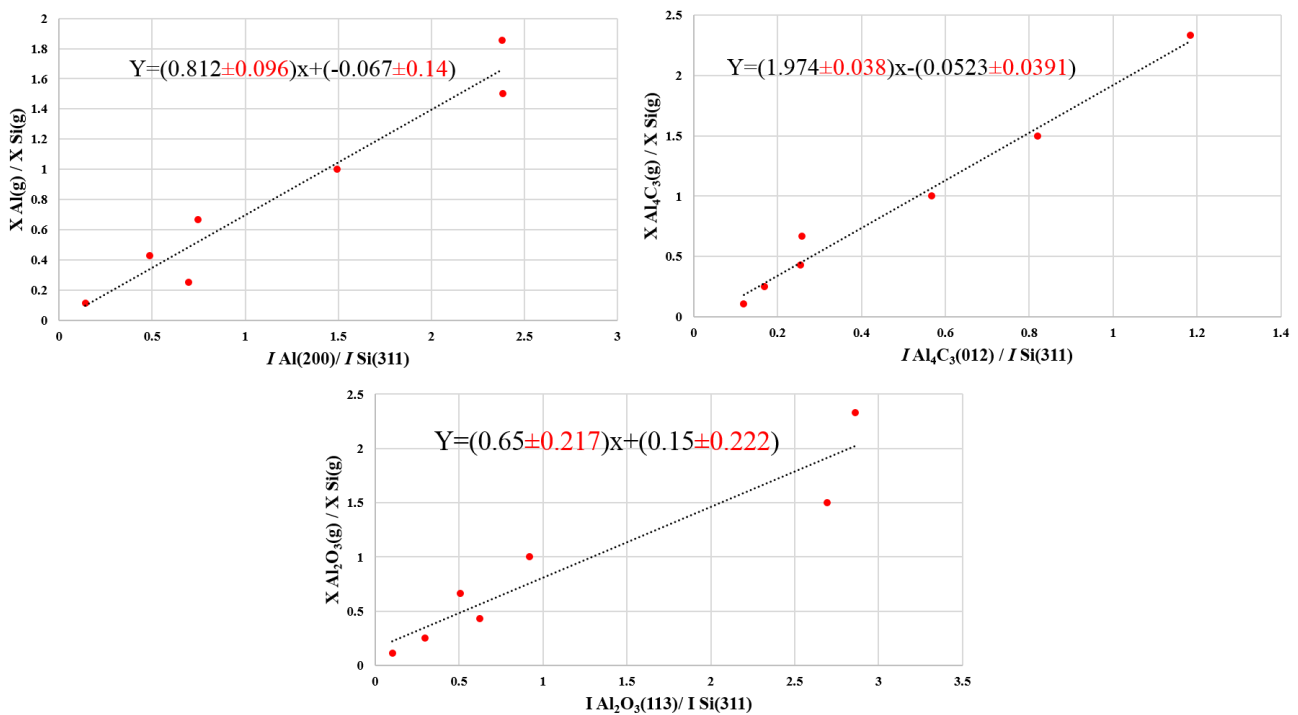
Fig. 21 Calibration curve used in the internal standard method calculation.

In this experiment, as a standard substance, Si was added, and a calibration curve (Fig. 21) was prepared by adding 10 wt% by weight ratio. By using this calibration curve, the weight ratio of Aluminum contained in the sample can be obtained by examining the ratio of the peak intensities of Si (311) and Al (200) of the sample. Therefore, in this experiment, a calibration curve of Aluminum, Alumina and Aluminum carbide was created and evaluated.

For error estimation, the standard uncertainties was estimated following this equations[88]:

$$Y = a + bx \qquad (17)$$

a: intercept of line on y-axis

b: the slope of the line

the residuals, $e_i(i=1,2,\ldots,n)$ are calculated as

$$e_i = y_i - a - bx_i \qquad (18)$$

and their root mean square value as

$$s = \sqrt{\frac{\sum_{i=1}^{n} e_i^2}{n-2}} \qquad (19)$$

when a straight line is fitted line to data, the standard uncertainties of intercept, a, and slope b are:

$$s_a = s \sqrt{\frac{\sum_{i=1}^{n} x_i^2}{D}} \qquad (20)$$

and

$$s_b = s \sqrt{\frac{n}{D}} \qquad (21)$$

where $D = n \sum_{i=1}^{n} x_i^2 - \left(\sum_{i=1}^{n} x_i \right)^2$ and n is number of samples

finally: $\qquad Y = (a \pm s_a) + (b \pm s_b) x \qquad (22)$

Chapter IV: Results and Discussion

This chapter is dedicated to the results and discussion of the experiences that have been made in these two research works. The first part of this chapter is devoted to results and discussion related to the optimziation of the process heating temperaure in order to achieve higher yield of aluminum production via carbothermal reduction of alumina. While the second part is dedicated to discuss the reuslts related to the effect of adding xoy-carbide materials and the optimization of its added amount in order to obtain a higher aluminum yield.

IV.1 Results and Discussion for Experimental Procedure #1
"Heating-Temperature Optimization"

IV.1.1. Heating-temperature Analysis

Figure 22 showed the different real-time temperature measured for the six samples during
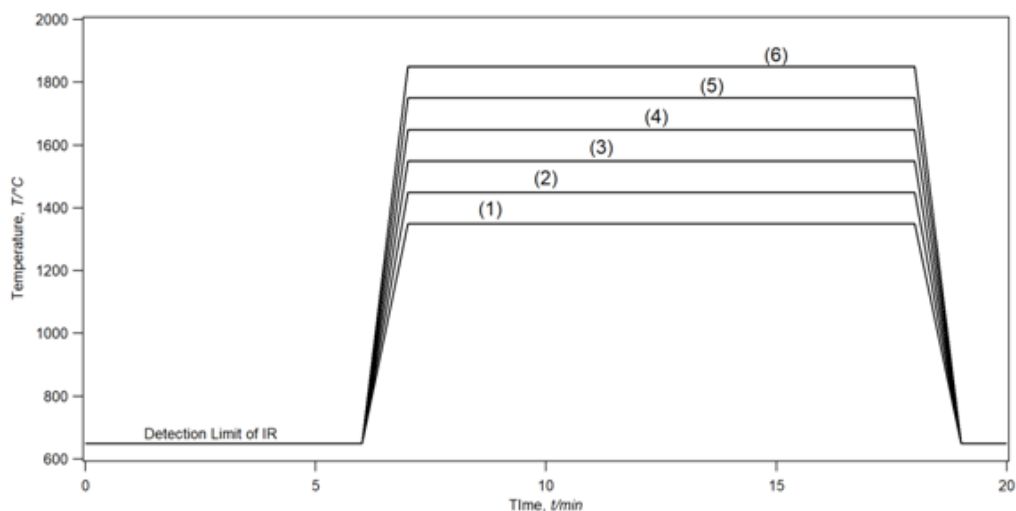
Fig. 22 The heating temperature profiles recorded for different samples measured at the surface of the crucible cap via an infrared thermometer during the reduction process. The recording starts at 650°C (923K) due to the limit in the detection range of the infrared thermometer from 650°C to 3500°C.

heating and compared to the same heating-time of 20 min. The temperature profile measured was quite stable for each sample and show a clear comparison of the heating-temperature variation. The heating-profile related to each temperature was pre-setup for each experiment before start heating while keeping the time lapse identical for all samples.

IV.1.2. Chamber Gas Analysis

Figure 23 shows a comparison of the Q-mass spectra between the background spectra and the various heating-temperature samples spectra's. The designated target for Q-mass spectra discussion, in this case, will be the mass peaks (m/Z=28) which correspond to the position of N_2/CO gasses. Reaching a lower N_2 background is crucial for a precise evaluation of CO gas evolution. N_2/CO background is illustrated in Figure 4 with a value of ion current below 3e-11 A. CO mass peak temporal variation represents a sign of occurrence for the reduction reactions. Therefore, the CO mass spectra variation will be used as a comparison factor between the various heating-temperature samples. Sample (1-4) shows a step increasing amount of CO gas by an increase in temperature from (1350ºC to 1650ºC). CO gas generation can be explained by starting of reaction (8) and (9) based on thermodynamic and phase diagram above discussions which show that reaction (8) starts at 1500ºC, however, our measured temperature was at the top of crucible cap, while inside crucible temperature can be estimated by ± 200ºC which is quite sufficient for generation of CO gas from reaction (8). Sample 5 with heating-temperature of 1750ºC exhibits the highest generated amount of CO gas while such amount decreased when heating up to 1850ºC in sample 6. To determine the origin of this difference in CO gas generation which can be translated to reactions occurrence, product analysis will be discussed in mass balance analysis.
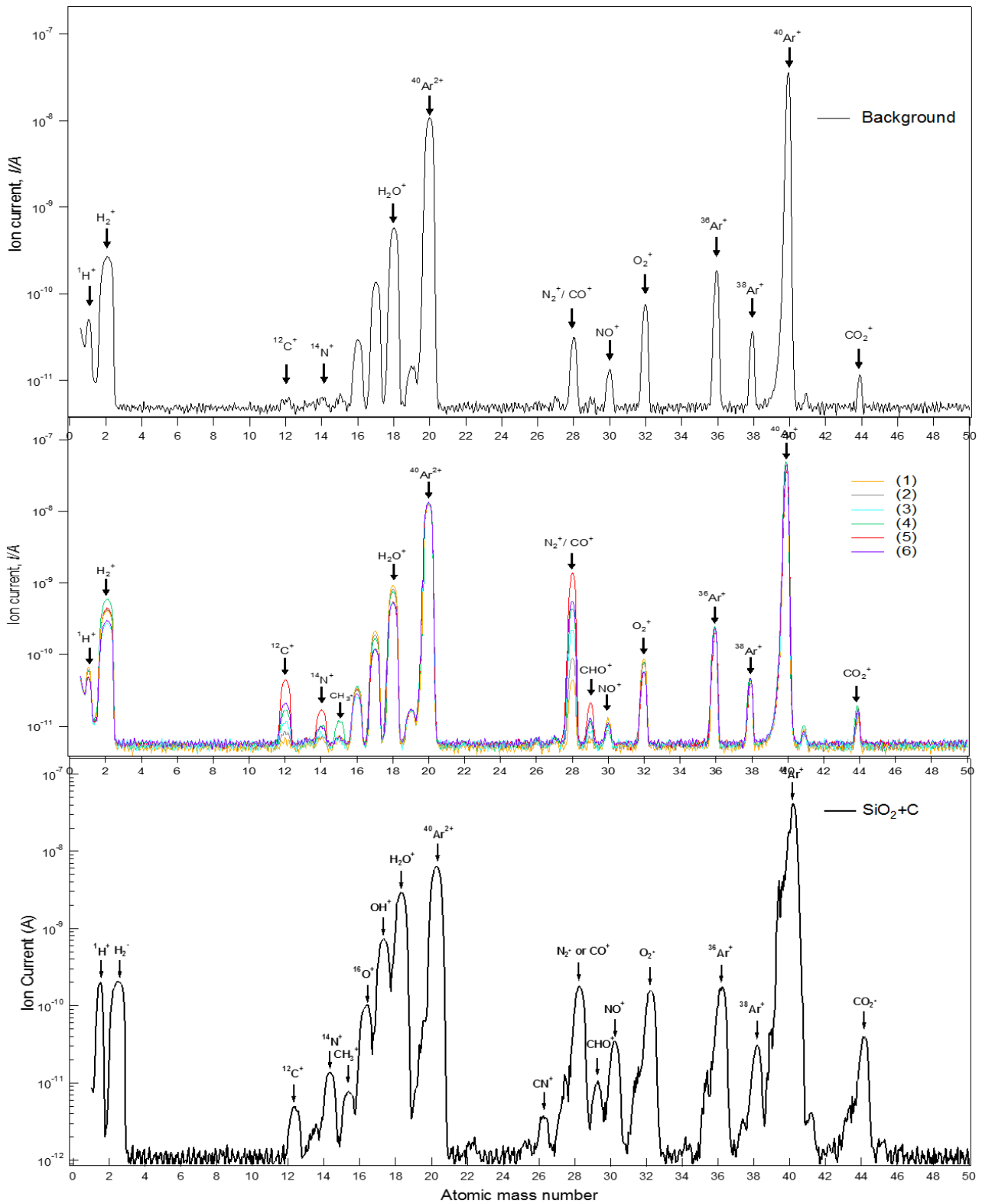
Fig. 23 Mass spectra of the chamber gases during the heating in case of six heating temperature profile. The amount of CO gas increased with increasing the temperature. However, the highest produced amount was achieved for a heating temperature of 1750 ℃ in the sample (5).

IV.1.3. Mass Balance Analysis

Table 4 illustrates the mass balance of the six samples including the amount of the input raw material, the amount of the obtained product which was calculated based on XRD analysis presented in Fig. 24, and the weight loss in the form of gas loss in our case. The yield of the produced Al material is defined as the molar ratio of the Al element in the product divided by the molar ratio of Al in the total input raw materials containing Al element. The input raw material consisted of Al_2O_3 and C with the ratio of (1:2) in all six samples. The analysis of table 8 indicates that in the sample (1-3) there was no production of Al due to the total conversion of the produced Al_2O from reaction (1), reacted with carbon to fulfill reaction (2) to generate Al_4C_3.
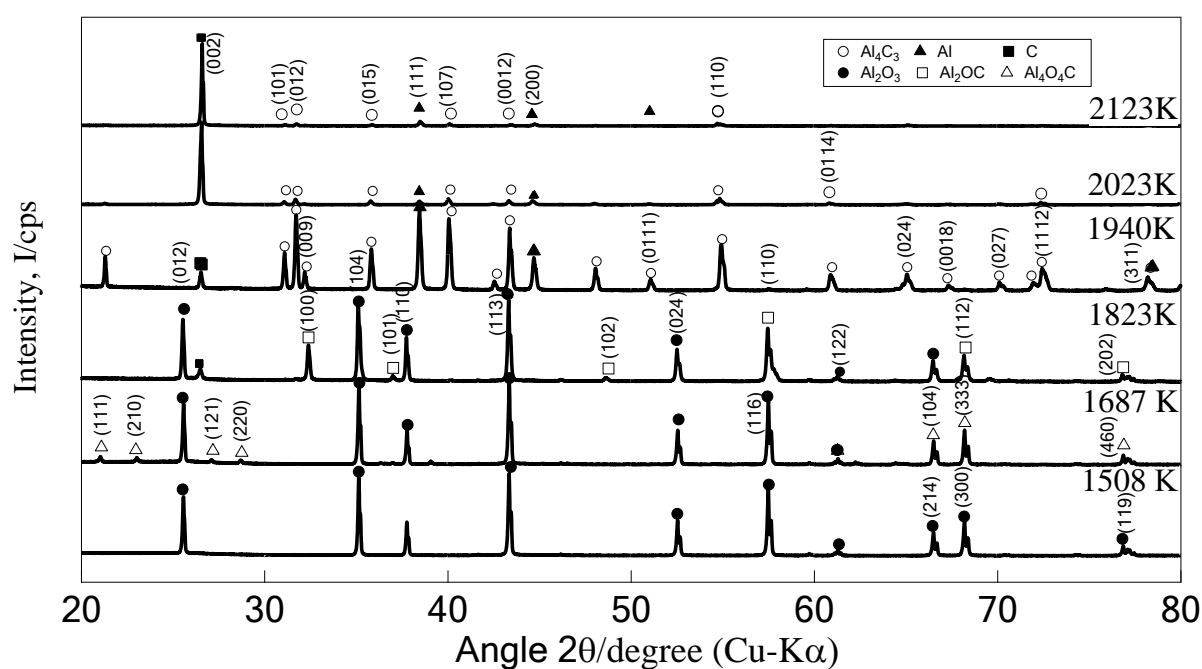
Fig. 24 X-ray diffraction patterns of obtained products for different heating-temperature profiles.

Table 8 Mass balance comparison between the six heating-temperatures samples shows that the highest yield of Al obtained in the reduction process corresponding to a heating temperature profile of 1750 ºC and measured at the cap of the crucible with an estimated error of ±200 ºC with inside crucible temperature. In order to facilitate the calculation, other oxy-carbide materials appearing in the XRD analysis were gathered in Al_4C_3.

		(1)		(2)		(3)		(4)		(5)		(6)
	(g)	(Al mol)	(g)	(Al mol)	(g)	(Al mol)	(g)	(Al mol)	(g)	(Al mol)	(g)	(Al mol)
Al_2O_3	5.15	0.10	5.15	0.10	5.15	0.10	5.15	0.10	5.15	0.10	5.15	0.10
C	1.83		1.83		1.83		1.83		1.83		1.83	
Total Input	6.98	0.10	6.98	0.10	6.98	0.10	6.98	0.10	6.98	0.10	6.98	0.10
Total Product	6.69	0.10	6.51	0.10	4.65	0.10	0.74	0.03	1.08	0.03	0.55	0.02
Al_2O_3	4.75	0.09	3.35	0.07	2.61	0.05	0.00	0.00	0.00	0.00	0.00	0.00
C	1.59		2.08		0.13		0.00		0.41		0.00	
Al	0.00	0.00	0.00	0.00	0.00	0.00	0.16	0.01	0.50	0.02	0.19	0.01
Al_4C_3	0.36	0.01	1.08	0.03	1.91	0.05	0.57	0.02	0.17	0.01	0.36	0.01
Lost Gas	0.28	0.00	0.47	0.00	2.33	0.00	6.24	0.07	5.90	0.07	6.43	0.08
Al_2O	0.00	0.00	0.00	0.00	0.00	0.00	2.45	0.07	2.45	0.07	2.80	0.08
CO	0.28		0.47		2.33		3.79		3.45		3.63	
Total Output	6.98	0.10	6.98	0.10	6.98	0.10	6.98	0.10	6.98	0.10	6.98	0.10
Al Yield (%)		0.00		0.00		0.00		6.01		18.35		6.97

The lower heating-temperature can explain these results which led to the minimum generation of Al_2O and Al_4C_3 via reactions (13) and (14) and not allowing the occurrence of the reaction (15) to produce Al. Furthermore, reaching a temperature of 1650ºC in sample allowed the generation of higher amount of Al_2O which its excess was detected via Q-mass which means left the crucible and Al_4C_3, in which their interaction led to generation of Al even with a low yield of 6%. Further increase of the heating temperature to 1750 ºC, engender a smooth and total occurrence of the reactions (12-15) which was awarded by obtaining the highest Al yield of 18%. An additional increase of the temperature for sample 6 led to opposite effect of lowering the generation of Al, and it is due to evaporation of Al_2O due to a higher temperature which means that 1750ºC represents the optimum heating temperature for obtaining a higher Al yield of the carbothermal reduction of alumina as shown in Fig.25..
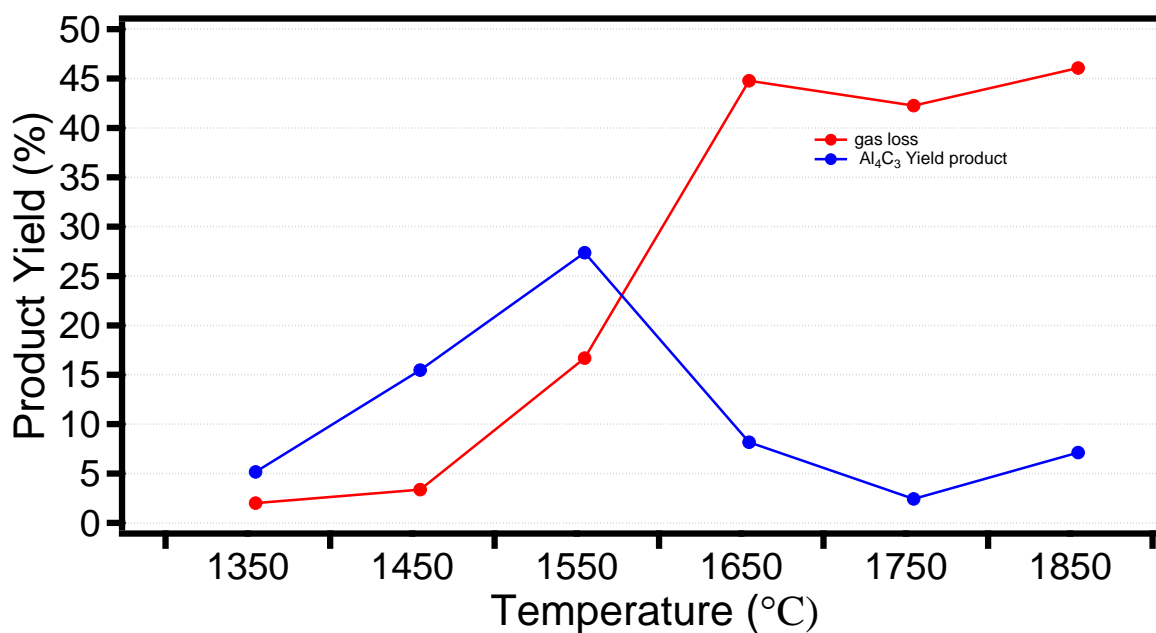
Fig.25 : Total Al_4C_3 and lost gas yield obtained from all samples.

Moreover, these results is backed up by the real images of the obtained product in the case of each sample as shown in Fig. 26
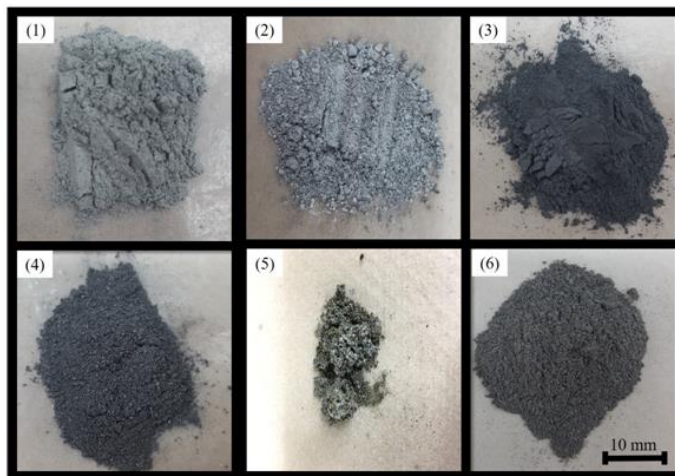
Fig. 26 Photos of the reduction product with six heating-temperature profiles. The color of the obtained product in each image exhibits approximately the containing elements of each occurred reaction.

In which sample (1) and (2) shows a light grey color due to remain of higher amount of unreacted Al_2O_3compared to sample (3) and (4) that shows a darker grey color due to

remain of unreacted carbon in the product and due to generation of sufficient amount of Al_4C_3 and Al in sample (4). While Al was generated with higher amount in the sample (5) which shows a metallic color corresponding to Al material presence. Sample (6) shows a darker grey color mainly due to uncreated carbon and generation of a higher amount of Al_4C_3which couldn't react to produce Al.

IV.1.4. Conclusion

The thermodynamic understanding of the overall reaction in the carbothermal reduction of alumina represented quite a useful technic to calculate the phase diagram of Al-O-C to determine the optimum heating temperature for obtaining a higher yield of Al theoretically. The estimation of the by-products generated during the reduction process such as Al_2O, CO, and Al_4C_3 is essential for the optimization and enhancement of the reduction process. The optimum heating temperature for a higher obtained yield of Al (18%) was determined to be around 1750°C in an argon atmosphere.

IV.2 Results and Discussion for Experimental Procedure #2
"carbide additive optimization"

IV.2.1 Chamber Gas Analysis

Figure 27 shows the temporal change of the relative mass peaks ($m/Z = 28$) in the case of 0.05 molar ratio additive of Al_4C_3. The peak with $m/Z = 28$ represents residual N_2 gas and CO gas evolution during heating which mainly occurred due to the carbothermic reduction of alumina. This increase of CO gas was mainly generated from carbothermal reduction because residual N_2 gas is regarded as constant background.

The gas losses of CO and Al_2O were estimated in Eqs. (23) and (24):

$$M(CO)_{mol} = P_{furnace}*k*V_{furnace} / R*T_{furnace} \tag{23}$$

$$M(Al_2O) = (W_{loss} - M(CO)mol * 28) / 70 \tag{24}$$

where R is gas constant, $P_{furnace}$, $V_{furnace,}$ and $T_{furnace}$ are the pressure (Pa), volume (m^3) and temperature (K) of the total gas in the furnace. k is the ratio of the mass peak intensity between CO and Ar in quadrupole mass spectroscopy at the end of the reaction as shown in Fig. 27. The increase of the peak intensity of $m/Z = 28$ was used to estimate the factor k, which will be used for the estimation of Al_2O gas release during the reduction.
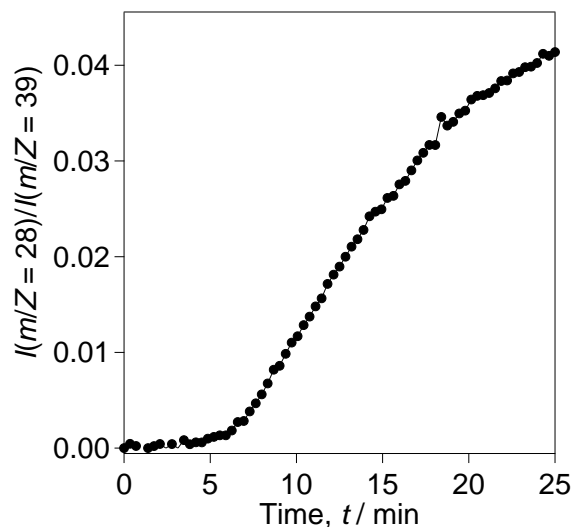
Fig. 27 Real-time evolution of the released CO gas during the reduction process analyzed by quadrupole mass spectrometry. The factor k was used for the calculation of Al_2O (mol) gas loss.

IV.2.2 Product Analysis

IV.2.2.1 Quantification of Products

Figure 28 shows the x-ray powder diffraction patterns for the milled products. An apparent effect of Al_4C_3 adding can be seen when comparing the different patterns related to progressive adding of Al_4C_3 molar ratio. A significant increase of the number and intensity of peaks corresponding to aluminum (Al) related to the progressive increase in mol% of Al_4C_3. The intermediate phases such as aluminum oxy-carbide (Al_4O_4C) appeared because of the incomplete reduction of Al_2O_3 to Al. The peaks related to Al_2O_3 and C represent the residual raw material due to incomplete reduction caused by gasses partial pressure inside the crucible or in case of only remains Al_2O_3 due to the exhaustion of carbon raw material. The carbon peaks can be explained by excess carbon powder or the graphite crucible. The excess of Al_4C_3 additives caused the decrease of Al content in the product as shown in Table 8.
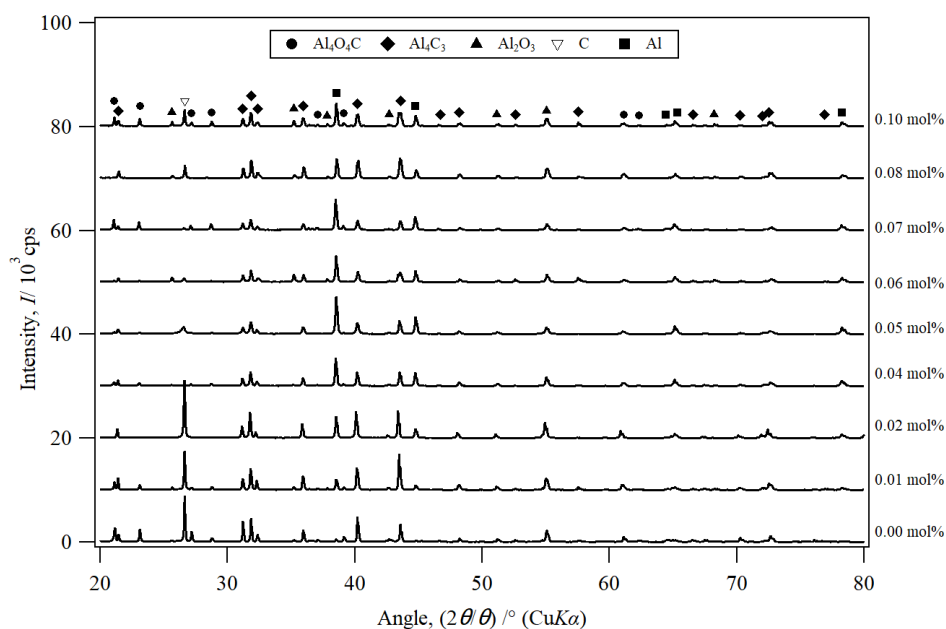
Fig. 28 X-ray diffraction patterns of obtained products in the case of various additives

(0 ~0.1 mol%) of Al_4C_3.

The peak intensities of the x-ray diffraction patterns were used for the quantification of the product using Eq. (15).

65

IV.2.2.2 Mass Balance

Table 8 shows the mass balance of the experimental results for the carbothermic reduction with the several different Al_4C_3 additives.

Table 8 Mass balance for input raw materials and output product solid and gas phases shows a significant increase in the yield of Al corresponding to adding 0.05 molar ratio of Al_4C_3 as compared with other ratios. This comparison revealed the positive effect of Al_4C_3 additive fo r the production of Al.

|		11		12		13		14		15	
		(g)	(Al mol)	(g)	(Al mol)	(g)	(Al mol)	(g)	(Al mol)	(g)	(Al mol)
Al_2O_3		14.800	0.290	14.800	0.290	14.800	0.290	14.800	0.290	14.800	0.290
C		5.210		5.210		5.210		5.210		5.210	
Al_4C_3		1.250	0.035	1.500	0.042	1.750	0.049	2.000	0.056	0.857	0.024
Total Input		21.260	0.325	21.510	0.332	21.760	0.339	22.010	0.346	20.867	0.314
Total Product		6.761	0.081	7.213	0.155	8.250	0.140	9.096	0.194	7.234	0.171
	Al	0.816	0.030	0.958	0.035	1.005	0.037	1.108	0.041	0.846	0.031
	Al_4C_3	0.749	0.021	0.612	0.017	0.086	0.002	0.274	0.008	0.974	0.027
	Al_4O_4C	0.894	0.0194	4.146	0.0901	4.002	0.0870	5.759	0.1252	4.340	0.0943
	Al_2O_3	0.516	0.010	0.639	0.013	0.682	0.013	1.045	0.020	0.931	0.018
	C	3.786		0.858		2.475		0.910		0.143	
Lost Gas		14.499		14.297		13.510		12.914		13.633	
	Al_2O	8.552	0.244	6.185	0.177	6.959	0.199	5.300	0.151	5.005	0.143
	CO	5.947		8.112		6.551		7.614		8.628	
Total Output		21.260	0.325	21.510	0.332	21.760	0.339	22.010	0.346	20.867	0.314
Al Yield (%)			9.301		10.692		10.986		11.869		9.979

		1		2		3		4		5	
		(g)	(Al mol)	(g)	(Al mol)	(g)	(Al mol)	(g)	(Al mol)	(g)	(Al mol)
Al_2O_3		14.800	0.290	14.800	0.290	14.800	0.290	14.800	0.290	14.800	0.290
C		5.210		5.210		5.210		5.210		5.210	
Al_4C_3		0.000	0.000	0.250	0.007	0.500	0.014	0.750	0.021	1.000	0.028
Total Input		20.010	0.290	20.260	0.297	20.510	0.304	20.760	0.311	21.010	0.318
Total Product		4.529	0.042	4.046	0.088	2.830	0.066	6.790	0.130	6.879	0.172
	Al	0.093	0.003	0.228	0.008	0.349	0.013	0.813	0.030	1.519	0.056
	Al_4C_3	0.177	0.005	0.000	0.000	0.271	0.008	0.171	0.005	0.142	0.004
	Al_4O_4C	0.756	0.0164	3.349	0.0728	1.836	0.0399	3.921	0.0852	4.686	0.1019
	Al_2O_3	0.876	0.017	0.348	0.007	0.292	0.006	0.518	0.010	0.525	0.010
	C	2.627		0.121		0.082		1.367		0.007	
Lost Gas		15.481		16.214		17.680		13.970		14.131	
	Al_2O	8.190	0.234	7.317	0.209	8.330	0.238	6.327	0.181	5.096	0.146
	CO	7.291		8.897		9.350		7.643		9.035	
Total Output		20.010	0.276	20.260	0.297	20.510	0.304	20.760	0.311	21.010	0.318
Al Yield (%)			1.187		2.842		4.251		9.681		17.693

	6		7		8		9		10	
	(g)	(Al mol)	(g)	(Al mol)	(g)	(Al mol)	(g)	(Al mol)	(g)	(Al mol)
Al_2O_3	14.800	0.290	14.800	0.290	14.800	0.290	14.800	0.290	14.800	0.290
C	5.210		5.210		5.210		5.210		5.210	
Al_4C_3	1.250	0.035	1.500	0.042	1.750	0.049	2.000	0.056	1.000	0.028
Total Input	21.260	0.325	21.510	0.332	21.760	0.339	22.010	0.346	21.010	0.318
Total Product	11.254	0.261	8.381	0.196	11.849	0.206	11.222	0.271	8.325	0.178
Al	1.013	0.038	0.983	0.036	1.116	0.041	1.057	0.039	1.443	0.053
Al_4C_3	0.631	0.018	0.656	0.018	0.296	0.008	2.735	0.076	0.000	0.000
Al_4O_4C	8.504	0.1849	5.736	0.1247	5.935	0.1290	5.935	0.1290	5.173	0.1125
Al_2O_3	1.083	0.021	0.847	0.017	1.383	0.027	1.383	0.027	0.635	0.012
C	0.023		0.159		3.119		0.112		1.074	
Lost Gas	10.006		13.129		9.911		10.788		12.685	
Al_2O	2.232	0.064	4.758	0.136	4.659	0.133	2.607	0.074	4.887	0.140
CO	7.774		8.371		5.252		8.181		7.798	
Total Output	21.260	0.325	21.510	0.332	21.760	0.339	22.010	0.346	21.010	0.318
Al Yield (%)		11.547		10.971		12.200		11.323		16.808

	16		17		18	
	(g)	(Al mol)	(g)	(Al mol)	(g)	(Al mol)
Al_2O_3	14.800	0.290	14.800	0.290	14.800	0.290
C	5.210		5.210		5.210	
Al_4C_3	0.857	0.024	1.125	0.031	1.125	0.031
Total Input	20.867	0.314	21.135	0.321	21.135	0.321
Total Product	9.182	0.204	8.808	0.193	8.503	0.198
Al	0.950	0.035	1.131	0.042	1.055	0.039
Al_4C_3	0.000	0.000	0.000	0.000	1.502	0.042
Al_4O_4C	6.849	0.1489	5.761	0.1252	4.207	0.0915
Al_2O_3	1.029	0.020	1.343	0.026	1.305	0.026
C	0.354		0.573		0.434	
Lost Gas	11.685		12.327		12.632	
Al_2O	3.841	0.110	4.479	0.128	4.326	0.124
CO	7.844		7.848		8.306	
Total Output	20.867	0.314	21.135	0.321	21.135	0.321
Al Yield (%)		11.205		13.031		12.156

Each column in Table 8 includes the amount of input raw materials, the product outputs, and weight loss gas. The Al product yield is defined as a molar ratio of Al element in the product and Al element in the input from Al_2O_3 raw material and Al_4C_3 additive.

Figure 29 shows Al yield as a function of the amount of Al_4C_3 additive. The total Al yield consists of Al element from two sources, Al_2O_3 raw material, and Al_4C_3 additives. The highest yield of Al with 17.69% was observed in the case with Al_4C_3 additive with

$Al_2O_3:Al_4C_3 = 1:0.05$ in molar ratio, while the lowest yield of 1.187% was observed in the case without Al_4C_3 additive. In the case of more than 0.05 mol Al_4C_3 additive, the total weight of solid product increased and the amount of intermediate product, Al_4O_4C and Al_4C_3, increased. This result indicates that the excess of Al_4C_3 additive caused the generation of the intermediate product, Al_4O_4C, and Al_4C_3.

The error was calculated using uncertainty equation [88] based on internal standard error equation.
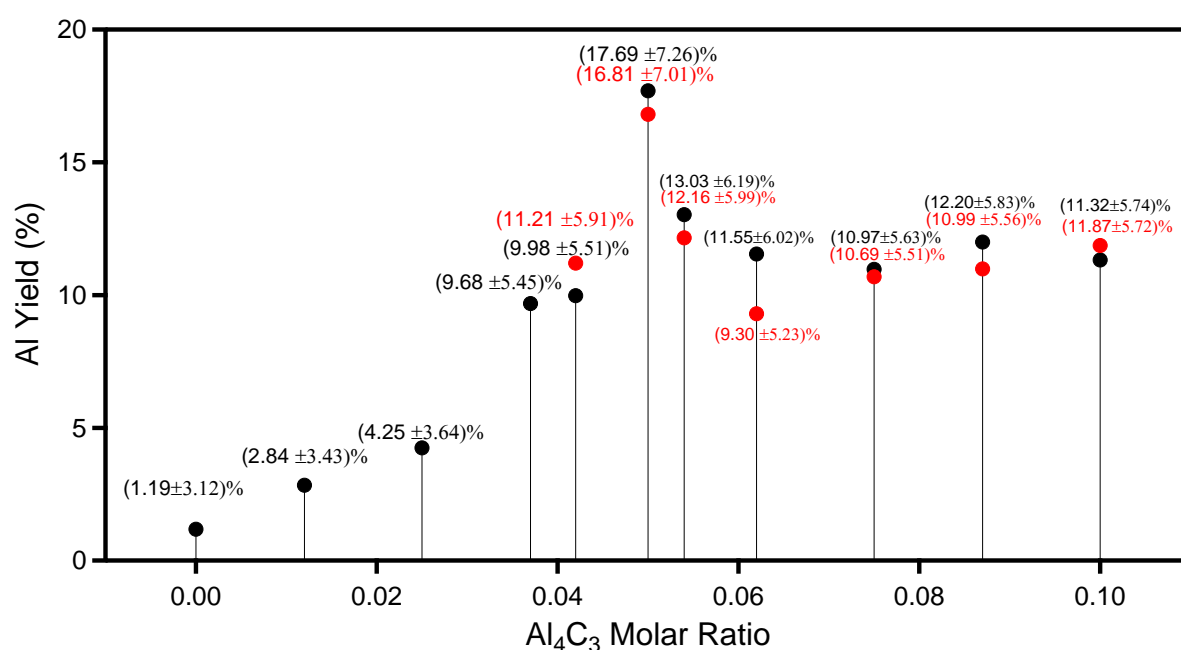
Fig. 29 Total Al yield obtained from all samples. The percentage of Al yield from Al_4C_3 was estimated. The highest Al yield was obtained in sample 5 where 0.05 mol% of Al_4C_3 was used.

If it is assumed that the whole Al_4C_3 additive was changed to Al metal perfectly, The experimental results in the range from 0.037 to 0.05 mol Al_4C_3 additive, however, showed higher gas lost yield than the others, and especially in sample 5 there no Al_4C_3 accur in product . Therefore, Al_4C_3 additive should have the effect to support the carbothermic reduction process from Al_2O_3 to Al.

This assumption was which confirm that Al total yield is generated through Al_2O_3 reduction. The Al yield from Al_2O_3 was much larger than that from Al_4C_3 additive. If the reaction of Eq. (12) causes the increase of the $P(Al_2O)/P(CO)$, the enhancement of the Al yield by Al_4C_3 additive can be explained by the gaseous phase diagram, Fig. 13. And Fig.30.

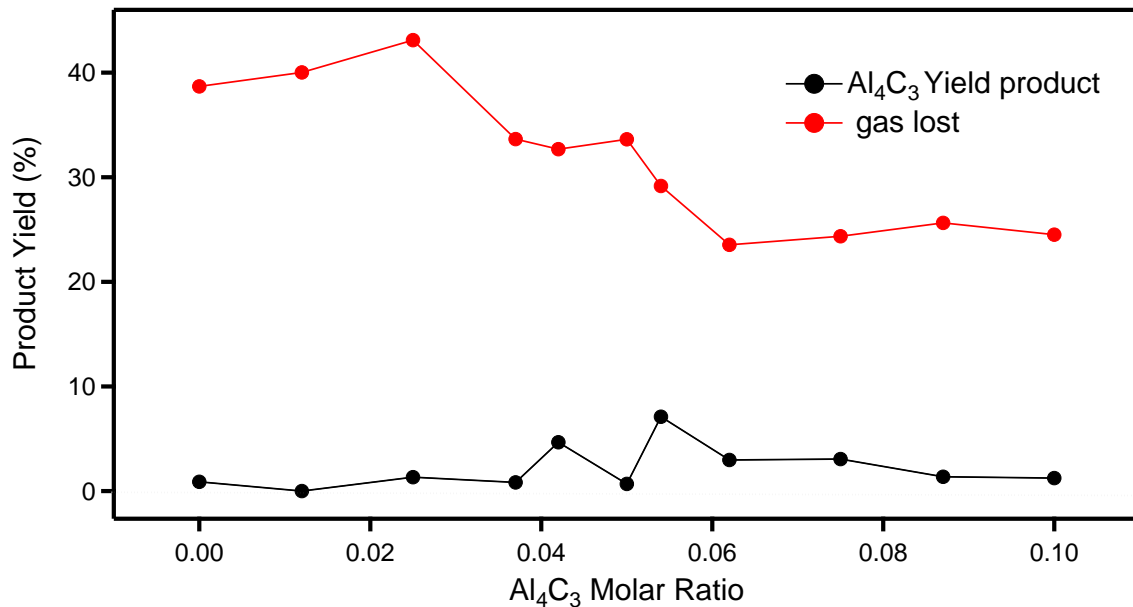**Fig. 30** Total Al_4C_3 and gas lost yield obtained from all samples

Although it is difficult to observe $P(Al_2O)$ directly in the capped carbon crucible because extracted Al_2O gas becomes solid below ~1000°C, our result strongly suggests that the possible explanation for the drastic change of Al yield by Al_4C_3 additive is due to the increase of the $P(Al_2O)/P(CO)$.

IV.2.2.3 SEM and EDS analyses

The top-view SEM images of the samples obtained by the heating of Al and carbon and Al4C3 additives are displayed in **Fig.31**. It can be observed in **Fig.31 (a)** that irregular grains exist in the sample. However, after introducing 0.05 mol% of Al_4C_3 additives **Fig. 31(b)**, both particle size and sphericity of the granules are remarkably improved by the appearance of spherical shape and the growth of particle size. In comparison, the products obtained from 0.05 mol% of Al_4C_3 and 0.1mol% appears to present the highest

individual sphericity **Fig. 31(c)**. Although near-spherical morphology also can be observed in the remaining sample, several hard agglomerates.
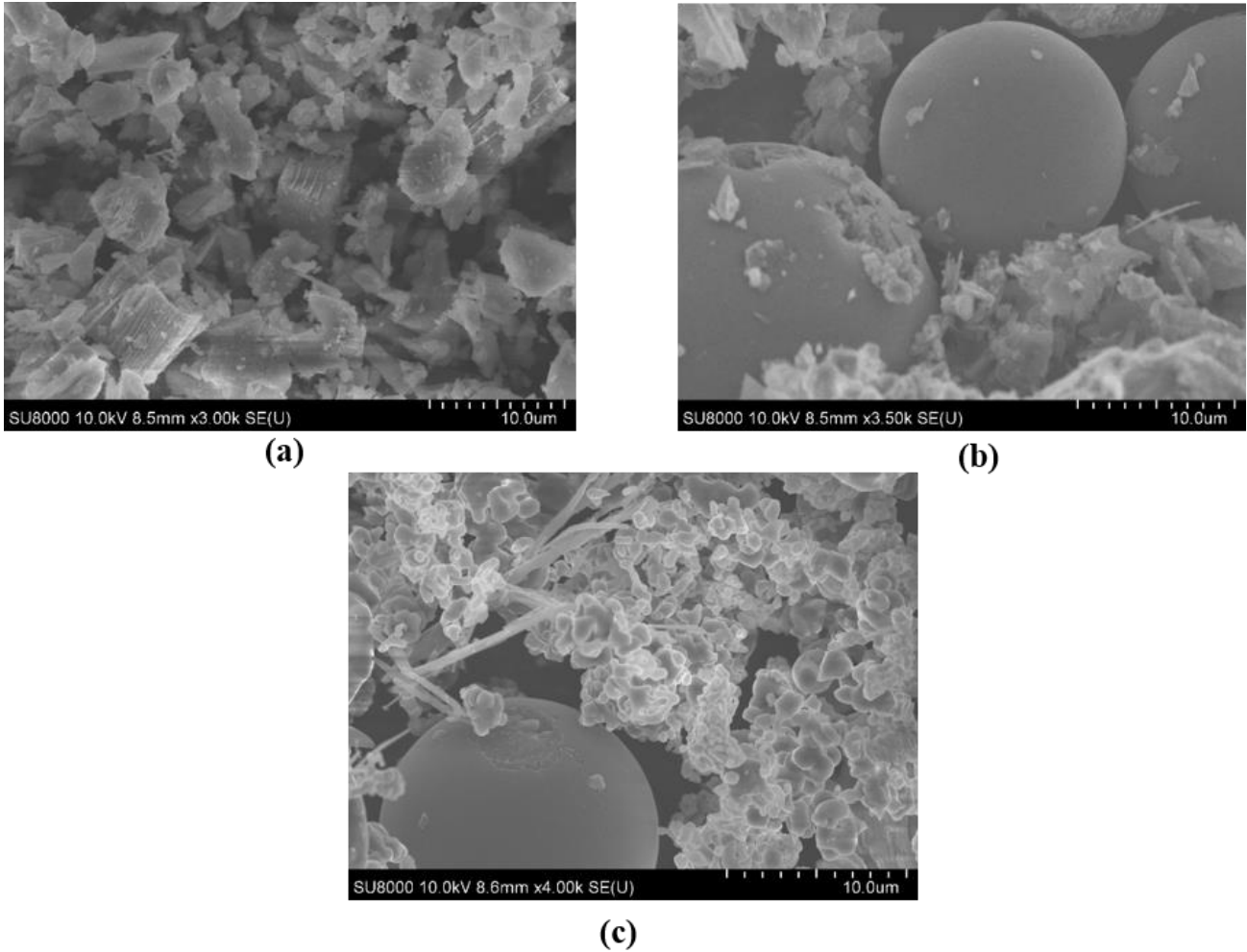
Fig.31 Morphology of the samples observed (**a**) sample 1 without Al_4C_3 additive (**b**) sample 5 with 0.05mol% of Al_4C_3 additive (**c**) sample 9 with 0.1mol% of Al_4C_3 additive.
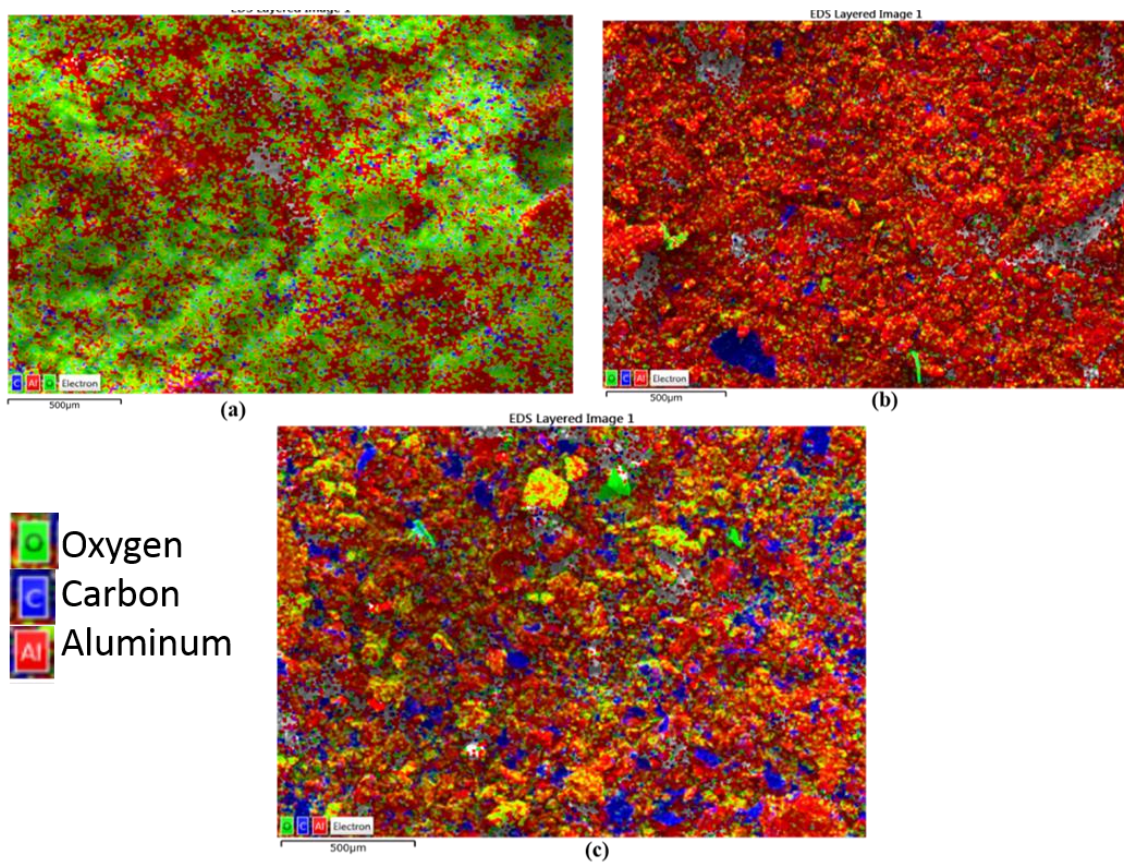
Fig.32 EDS mapping of particles morphology (**a**) sample 1 without Al_4C_3 additive (**b**) sample 5 with 0.05mol% of Al_4C_3 additive (**c**) sample 9 with 0.1mol% of Al_4C_3 additive.500µm

The EDS mapping **Fig.32** confirm that the apperance sperical shape is Al particules observed on the surface, for Al has changed to segragation and sometimes despersion.
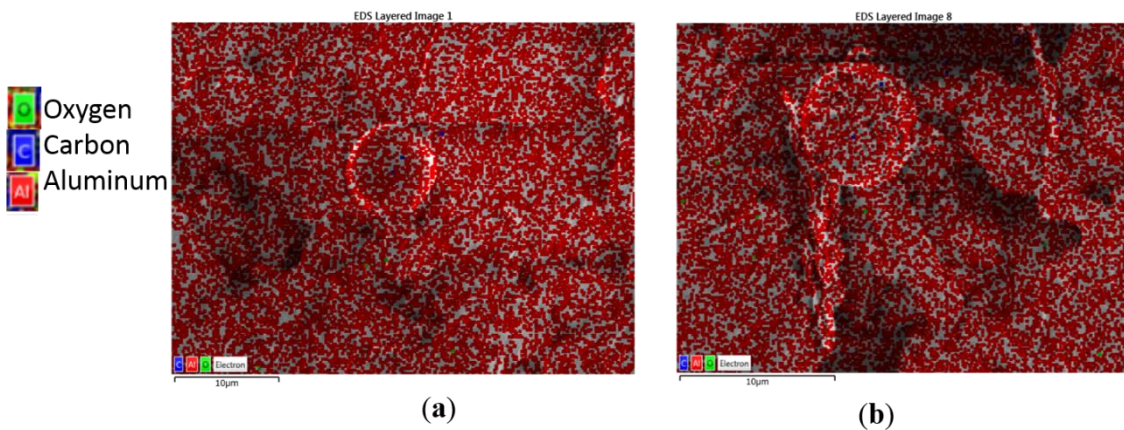
Fig.33 EDS mapping of particles morphology (**a**) sample 5 with 0.05mol% of Al_4C_3 additive (**b**) sample 9 with 0.1mol% of Al_4C_3 additive. 10µm

IV.2.3. Conclusion

We calculated the Al-O-C gaseous phase diagrams for the carbothermic reduction of Al. This phase diagram suggests that importance of the ratio of partial pressure $P(Al_2O)/P(CO)$ to improve the Al yield for the carbothermic reduction process of Al_2O_3. The adding of Al_4C_3 additive to raw material, Al_2O_3 and carbon, was proposed as a way to increase the ratio of partial pressure $P(Al_2O)/P(CO)$. The effect of Al_4C_3 additive on the carbothermic reduction of Al_2O_3 was investigated experimentally. In the case without Al_4C_3 additive, the Al yield was only 1.19 %, while, in the case of adding Al_4C_3 additive with $Al_2O_3{:}Al_4C_3 = 1{:}0.05$ in molar ratio, the Al yield increased drastically by 15 times up to 17.69 %.

References

[1] F. Habashi, G.E. Totten, M. Dekker, and D.S. Mackenzie, Handbook of aluminum: alloy production and minerals Alloy production and materials manufacturing ed. Vol. 2. 2003: Inc. 1-45.

[2] A.R. Hind, S.K. Bhargava, and S.C. Grocott, The surface chemistry of Bayer process solids: a review Colloids and Surfaces A: Physicochem. Eng, 1999. 146: p. 359-374.

[3] E. Schatzberg, Symbolic Culture and Technological Change: The Cultural History of Aluminum as an Industrial Material vol4, pp. 226-271(2003).

[4] L. Edwards, the History and Future Challenges of Calcined Petroleum Coke Production and Use in Aluminum Smelting Vol 67, pp 308–321 (2015).

[5] History Of Aluminum: facts and information on aluminum. 2006 [cited 2009 11/11/2009]; http://www.historyofaluminum.com/usage.php. aluminiumleader.com/history/industry history.

[6] P. A. Plunkert, Aluminum in 1994 - USGS Mineral Resources Program, minerals.usgs.gov/minerals/pubs/commodity/aluminum.

[7] V. Vorotnikov, Soft prices and slack demand force one of the world's largest aluminum producers to seek efficiency improvements, October 2015, Engineering & Mining Journal.

[8] Nappi, Carmine, Director for Industry Analysis, Alcan Inc., "China's Aluminum Industry, An Update," 72nd Annual Meeting of the Aluminum Association, Naples, FL, October 3-4, 2005.

[9] H.G. Fung, Qingfeng "Wilson" Liu, Yiuman Tse, The Journal of Futures Markets, Vol. 30, No. 12, 1192–1209 (2010).

[10] A life-cycle model of Chinese grid power and its application to the life cycle impact assessment of primary aluminum, http://www.world-aluminium.org

[11] M. Richard, Levine, the Mineral Industry of Russia, U.S. Geological Survey Minerals Yearbook –(1999).

[12] A. Toscano, F. Bilotti, F. Asdrubali, C. Guattari, L. Evangelisti and C. Basilicata, Recent Trends in the World Gas Market: Economical, Geopolitical and Environmental Aspects, Sustainability, 8, 154,(2016).

[13] D. Starta, A. Poddar, J. Alberich, A.T. Kearney, How GCC smelters Can continue growing profitably.

[14] Metals & Electronics, 2016 Global demand for semi-finished aluminum products in 2016, by sector: https://www.statista.com/statistics/280983/share-of-aluminum-consumption-by-sector.

[15] McCoy JP: Bauxite Processing and the Role of Less Developed Countries. The Social Science Journal 1989, 26(4):399-413.

[16] W. Liu, Yang J, Xiao B: Review on Treatment and Utilization of Bauxite

Residues in China. International Journal of Mineral Processing, UNSW Materials Science and Engineering School 83 93(3-4):220-231, (2009).

[17] V.M. Sglavo, S. Maurina, A. Conci, A. Salviati, G. Carturan, G. Cocco: Bauxite 'Red Mud' in the Ceramic Industry. Part 2: Production of Clay-based Ceramics. Journal of the European Ceramic Society, 20(3):245-252, (2000).

[18] V.M. Sglavo, R. Campostrini, S. Maurina, G. Carturan, M. Monagheddu, G. Budroni, G. Cocco: Bauxite 'Red Mud' in the Ceramic Industry. Part 1: Thermal Behaviour. Journal of the European Ceramic Society, 20(3):235-244, (2000).

[19] PH. Suman and M.O. Orlandi, Influence of processing parameters on nanomaterials synthesis efficiency by a carbothermal reduction process. J. Nanopart Res 13(5):2081–2088, (2011).

[20] E.Myrhaug and H. Tveit, , "Material balances of trace elements in the ferrosilicon and silicon processes", 58th Electric Furnace Conference, Orlando, Florida, November (2000).

[21] R. Benioub, M. Adnane, A. Boucetta, A. Chahtou, H. Kobatake, Y. Furuya and K. Itaka: *Journal of New Technology and Materials*,Vol. 7 (2017), 90-96.

[22] R. Benioub, A. Boucetta, A. Chahtou, S. M. Heddadj, M. Adnane, Y. Furuya and K. Itaka: Mater. Trans. 57 (2016), 1930-1935.

[23] A. Boucetta, R. Benioub, A. Chahtou, S. M. Heddadj, T. Ogasawara, Y. Furuya, S. Hamzaoui and K. Itaka: Mater. Tran, JIM. 57(2016) 1936-1944.

[24] M. A. Rhamdhani, M. A. Dewan, G. A. Brooks, B. J. Monaghan, and L. Prentice: Proc. Rev. Min. Proc. Extra Metall. **122** (2013) 87-104.

[25] J. P. Murray: J. Sol. Energy Eng. **123** (2001) 125-132.

[26] T. E. Norgate, S. Jahanshahi, W.J. Rankin: J. Clean. Prod. **15** (2007) 838-848.

[27] E. Balomenos, D. Panias, L. Paspaliaris, B. Friedrich, B. Jaroni, A. Steinfeld, E.Guglielmini, M. Halmann, M. Epstein, I. Vishnevsky: Proc. EMC (2011) 729-743.

[28] E. Balomenos, I. Gianopoulou, D. Panias, I. Paspaliaris: J. Metalurgija **15** (2009) 203 217.

[29] M. J. Bruno: Proc. Light Metals TMS. (2003) 395-400.

[30] R. J. Fruehan, Y. Li, and G. Carkin: J. Metall. Mater. Transac. B, **35** (2004) 617-623.

[31] P. Lefort, D. Tetard and P. Tristant: J. Euro. Ceram. Soc. **12** (1993) 123-129.

[32] J. H. Cox and L.M. Pidgeon: Can. J. Chem. **41** (1963) 671-683.

[33] M. Halmann, A. Ferai, A. Steinfeld: Energy **32** (2007) 2420–2427.

[34] M. Halmann, A. Steinfeld, M. Epstein, E. Guglielmini, I. Vishnevetsky: Conf. ECOS. (2012).

[35] M. Krusai, M.E. Galvez, M. Halmann, and A. Steinfeld: J. Metall. Mater. Transac. B, **42** (2011) 254-260.

[36] Y. Qing-chun, Y. Hai-bin, Z. Fu-long, Zhang Han, W. Chen, L. Da-chun, Y. Bin: J. Cent. South Univ. **19** (2012) 1813-1816.

[37] J. M. Lihrmann: J. Europ. Ceram. Soc. **28** (2008) 633-642.

[38] J. M. Lihrmann: J. Europ. Ceram. Soc. **28** (2008) 649-656.

[39] K.Itaka, T. Ogasawara. A. Boucetta, R. Benioub, M. Sumiya, T. Hashimoto, H. Koinuma, and Y. Furuya, "journal of physics: conference series, Vol 596, pp. 012015, **(2015)**.

[40] JP. Murray: Aluminium Production Using High-temperature Solar Process Heat. Solar Energy 1999, 66(2):133-142.

[41] M.J. Bruno: Production of Aluminum-Silicon Alloy and Ferrosilicon and Commercial Purity Aluminum by the Direct Reduction Process, Alcoa Technical Report, ALCOA, (1983), pp. 417ff. 3. K.

[42] K.L. Lee, H.Y. Hsu, M.L. You, et al. Highly Sensitive Aluminum-Based Biosensors using Tailorable Fano Resonances in Capped Nanostructures, Scientific reports, (2017);7:44104.

[43] S.A. Maier, Springer-Verlag, New York, (2007).

[44] J. Homola, S.S. Yee, G. Gauglitz, Surface plasmon resonance sensors: review. Sens Actuator B-Chem. (1999);54(1-2):3–15.

[45] J. Homola. Surface Plasmon Resonance Sensors for Detection of Chemical and Biological Species. Chem Rev. (2008);108(2):462.

[46] H. Raether. Springer Tracts Mod Phys. (1988);111.

[47] J.N. Anker, W.P. Hall, O. Lyandres, Biosensing with plasmonic nanosensors. Nat Mater. (2008);7:442.

[48] H. Im, S.H. Lee, N.J. Wittenberg, Template-Stripped Smooth Ag Nanohole Arrays with Silica Shells for Surface Plasmon Resonance Biosensing. ACS Nano. (2011);5(8):6244.

[49] C.V. Tejero, S. Herranz, A. Bellingham, Passivated Aluminum Nanohole Arrays for Label-Free Biosensing Applications. ACS Appl Mater Inter. (2014);6(2):1005.

[50] J.L. Skinner, L.L. Hunter, A.A. Talin, Large-Area Subwavelength Aperture Arrays Fabricated Using Nanoimprint Lithography. IEEE T Nanotechnol. (2008);7(5):527.

[51] M. Norek , M. Włodarski, P. Matysik, UV plasmonic-based sensing properties of aluminum nanoconcave arrays. Curr Appl Phys. (2014);14(11):1514.

[52] Q. Y. Chun, Y. Hai-Bin, Z. Fu-Long, Carbothermic reduction of alumina with carbon in vacuum. Journal of Central South University. (2012);19(7):1813.

[53] J. Safarian. PhD thesis, NTNU, Trondheim, Norway, (2007).

[54] R. Kononov, O. Ostrovski, S. Ganguly. Carbothermal Reduction of Manganese Oxide in Different Gas Atmospheres. Metall Mater Trans B. (2008);39(5):662-668.

[55] Y.F. Bin, Y. Bin, D. Yong-Nian. The Ch. J. of Nonferrous Metals. (2011);21:1748.

[56]   M. Yastreboff, O. Ostrovski, S. Ganguly, Effect of Gas Composition on the Carbothermic Reduction of Manganese Oxide. ISIJ Int. (2003);43(3):161-165.

[57]   M. Yastreboff. PhD thesis, University of New South Wales, Sydney, Australia, (2001).

[58]   M. Halmann, A. Frei, A. Steinfeld. Vacuum Carbothermic Reduction of Al_2O_3, BeO, MgO-CaO, TiO_2, ZrO_2, HfO2 + ZrO_2, SiO_2, SiO_2 + Fe_2O_3 and GeO_2 to the Metals. A Thermodynamic Study. Mineral Processing and Extractive Metallurgy Review. (2011);32(4):247–266.

[59]   M.A. Rhamdhani. G.A. Dewan, J.B. Brook, Alternative Al production methods. Mineral Processing and Extractive Metallurgy. (2013);122:87.

[60]   R. Kononov, O. Ostrovski, S. Ganguly. Carbothermal Solid State Reduction of Manganese, ISIJ Int. (2009);49(8):1099–1106.

[61]   R. Kononov, O. Ostrovski, S. Ganguly, Carbothermal Solid State Reduction of Manganese, ISIJ Int. (2009);49(8):1107–1114.

[62]   R. Kononov, O. Ostrovski, S. Ganguly. Ganguly. Carbothermal Solid State Reduction of Manganese Ores: 3. Phase Development. ISIJ Int.(2009);49(8):1115–1122.

[63]   O. Ostrovski, S.E. Olsen, M. Tangstad, Kinetic Modelling of MnO Reduction from Manganese Ore. Can Metall Q. (2002);41(3):309–318.

[64]   O. Ostrovski, S.W. Thompson. Ferritic Microstructures in Continuously Cooled Low- and Ultralow-carbon Steels. ISIJ Int.(1995);35(8):937–945.

[65]   R.H. Eric, E. Burucu, Miner Eng. (1992);5:795.

[66]   V.N. Misra, Proc 14th CMMI Congress, the Institution of Mining and Metallurgy, Edinburgh, Scotland, (1990), 39p.

[67]   M. Kruesi, M.E. Galvez, M. Halmann, Solar Aluminum Production by Vacuum Carbothermal Reduction of Alumina—Thermodynamic and Experimental Analyses. Metall Mater Trans B. (2011);42(1):254–260.

[68]   G. Akdogan, R.H. Eric, Int J Mater Prod Technol. (1993);8:29.

[69]   G Akdogan, R.H. Eric. Miner Eng. (1994);7:633.

[70]   G. Akdogan, R.H. Eric. Kinetics of the solid-state carbothermic reduction of wessel manganese ores. Metall Mater Trans B. (1995);26(1):13.

[71]   R.J. Fruehan, G. Carkin, Metall Mater Trans B. (2004);35:1011.

[72]   O. Holta, S.E. Olsen. Proc Electric Furnace. Conf, Vol. 43, Iron & Steel Society, Warrendale, PA, (1986). 273 p.

[73]   K. Tereyama, M. Ikeda, Trans Jpn Inst Met. (1985);26:108.

[74]   W.J. Rankin, J.R.Wynnyckyj, Kinetics of reduction of MnO in powder mixtures with carbon. Metall Mater Trans B. (1997);28(2):307.

[75]   W.J. Rankin, V. Deventer, JSJ. J S Afr Inst Min Metall. (1980);80:239.

[76]   N. Hashimoto, H. Yoden, K. Nomura, Preparation of Aluminum Nitride Powder from Aluminum Polynuclear Complexes. J.Am.Ceram.Soc, (1991);74(6):1282–

1286.

[77]   S. Duan, X. Chen, B. Yang, Calculation of interaction of AlCl, $AlCl_2$ and $AlCl_3$ on Al_4C_3 (001) Al_4CO_4 (001) and Al_2CO (001) planes. J. Cent South Uni. (2015);22(1):43–58.

[78]   M. Heyrman, C. Chatillon, Thermodynamics of the Al –C–O Ternary System I. Second and Third Law Critical Analysis of Oxycarbide Enthalpies from Vapor Pressure Determinations. J. Electrochemical Society. (2006);153:e119.

[79]   J. Li, G. Zhang, D. Liu, Low-temperature Synthesis of Aluminium Carbide. ISIJ Int. (2011);51(6):870.

[80]   T. Yamakawa, J. Tatami, T. Wakihara, Synthesis of AlN Nanopowder from γ Al_2O_3 by Reduction–Nitridation in a Mixture of NH3–C3H8. JAm Ceram Soc. (2006);89(1):171.

[81]   H. Yokokawa, S. Yamauchi, T. Matsumoto, Thermodynamic database MALT2 and its applications to high temperature materials chemistry. Acta Thermo. (1994);245:45

[82]   E. Balomenos, D. Panias, and L. Paspaliaris: Proc. Rev. Min. Proc. Extra Metall. **32** (2011) 69-89.

[83]   H. Yokokawa, S. Yamauchi, T. Matsumoto: Calphad **26** (2002) 155-166.

[84]   William T. Choate, BCS, John A. S. Green, U.S. Aluminum Production Energy Requirements: Historical Perspective, Theoretical Limits, and New Opportunities, (2003) p1-13.

[85]   M. Bruno, Aluminum carbothermic technology comparison to Hall-Heroult process. In Light Metals; TMS: Warrendale, PA, USA, (2003); pp. 395–400.

[86]   U. Bossel, Well-to-Wheel Studies, Heating Values, and the Energy Conservation Principle. European Fuel Cell Forum, (2003); PP1-5.

[87]   M. Obaidat, A. Al-Ghandoor, P. Phelan, R. Villalobos and A. Alkhalid, Energy and Exergy Analyses of Different Aluminum Reduction Technologies, Sustainability (2018), 10, 1216

[88]   L. Kirkup, B. Frenkel, an introduction to uncertainty in measurement (2006), pp50-72